An Eigenvalue-Moment-Ratio Approach to Blind Spectrum Sensing for Cognitive Radio Under Sample-Starving Environment

Lei Huang, *Member, IEEE*, Jun Fang, *Member, IEEE*, Kefei Liu, Hing Cheung So, *Senior Member, IEEE*, and Hongbin Li, *Senior Member, IEEE*

***Abstract*—Eigenvalue-based methods have been widely investigated for multiantenna blind spectrum sensing in cognitive radio (CR). However, most of them are formulated in the framework of maximum likelihood (ML) estimation, which is optimal only when the number of samples is much larger than the number of antennas. In relatively small-sample scenarios where the number of antennas is comparable in magnitude to the number of samples, their optimality cannot be guaranteed. Based on the random matrix theory (RMT), an eigenvalue moment ratio (EMR) approach is proposed for spectrum sensing. As the distribution of the EMR statistic in the absence of signals can be precisely determined by the RMT, this approach is able to reliably predict the theoretical threshold. Moreover, as the EMR detector is developed from the RMT perspective and utilizes all the signal eigenvalues for detection, it can be superior to state-of-the-art detection algorithms, particularly for relatively small samples. Furthermore, we derive the asymptotic distribution of the EMR statistic in the presence of signals and analyze the theoretical detection probability of the EMR approach. Additionally, the EMR statistic is calculated via the Frobenius inner product and matrix trace operations instead of the eigenvalue decomposition (EVD), which offers computational efficiency. Simulation results are presented to illustrate the superiority of the EMR approach and confirm our theoretical calculation.**

***Index Terms*—Cognitive radio (CR), moment of eigenvalues, random matrix theory (RMT), spectrum sensing.**

Manuscript received June 24, 2014; revised August 7, 2014; accepted September 15, 2014. Date of publication September 19, 2014; date of current version August 11, 2015. This work was supported in part by a grant from the National Natural Science Foundation of China (NSFC)/Research Grants Council (RGC) of Hong Kong (NSFC/RGC) Joint Research Scheme sponsored by the RGC; by the NSFC under Project (N_CityU 104/11, 61110229/61161160564), Grant 61222106, and Grant 61171187; and by the Shenzhen Kongqie talent Program under Grant KQC201109020061A. The review of this paper was coordinated by Dr. E. K. S. Au.

L. Huang is with the Department of Electronic and Information Engineering, Harbin Institute of Technology Shenzhen Graduate School, Shenzhen 518055, China (e-mail: dr.lei.huang@ieee.org).

J. Fang is with the National Key Laboratory of Science and Technology on Communications, University of Electronic Science and Technology of China, Chengdu 611731, China (e-mail: JunFang@uestc.edu.cn).

K. Liu is with the Department of Computer Science and Engineering, Arizona State University, Tempe AZ 85281 USA (e-mail: kefei.liu.1@asu.edu).

H. C. So is with the Department of Electronic Engineering, City University of Hong Kong, Kowloon, Hong Kong (e-mail: hcso@ee.cityu.edu.hk).

H. Li is with the Department of Electrical and Computer Engineering, Stevens Institute of Technology, Hoboken, NJ 07030 USA (e-mail: Hongbin.Li@stevens.edu).

Color versions of one or more of the figures in this paper are available online at http://ieeexplore.ieee.org.

Digital Object Identifier 10.1109/TVT.2014.2359217

I. Introduction

INCREASING demand of high-data-rate communication has aggravated the severe situation of spectrum deficiency, which results from the policies of fixed spectrum allocation [1]. To alleviate the spectrum deficiency, cognitive radio (CR) [2] has been deemed as a potential paradigm for future communications. In a CR network, a secondary user (SU) is allowed to borrow the frequency channels preassigned to the primary users (PUs) by the government when they are inactive. Once the PUs become active again, the SU is required to vacate its occupied channels to the PUs as soon as possible. This scheme of dynamic spectrum access is able to dramatically enhance the spectral usage. To maximize the spectral utilization and minimize the harmful interference to the PUs, the SU needs to reliably detect the PUs.

In traditional techniques for spectrum sensing, such as cyclostationary detection [3], matched filtering [4], and energy detection [5], it is assumed that full or partial knowledge of the PU signal characteristics, the channel responses of the PUs, and/or the noise power are available at the CR receiver. However, such knowledge might be unavailable in a realistic CR network.

Numerous blind spectrum sensing methodologies that require no primary signal information or noise variance have been proposed in the literature. Usually, they utilize the correlation structure inherent in the received data for detection, which results from the multipath propagation and/or oversampling of the primary signals for a single-antenna receiver or the deterministic channel during the sensing period for a multiantenna receiver. In [6], the covariance absolute value (CAV) detector is heuristically derived from the test of the identity structure of covariance matrix against its general correlated alternative. As a matter of fact, the correlation structure among the sample covariance matrix (SCM) leads to the significant spread out of eigenspectrum, providing a good indicator for the primary signals. Consequently, eigenvalue-based sensing schemes have received much attention [7]–[14]. Derived in the framework of a generalized likelihood ratio (GLR) test, the eigenvalue arithmetic-to-geometric mean (AGM) [13], [15], [16] and GLR [9], [17] detectors are able to reliably identify correlated signals embedded in additive independent and identically distributed (i.i.d.) noise. Unlike the AGM algorithm, the variants of the GLR method, i.e., the rank-1 GLR [9] and rank-d GLR [17], rely on the *a priori* knowledge of the primary signal number

and, hence, are more accurate than the AGM approach. Here, d is the number of primary signals. Moreover, it has been shown in [12] that the rank-1 GLR method asymptotically outperforms the maximum–minimum eigenvalue (MME) detector [8], which is heuristically derived for single-source detection. However, the number of primary signals may be unknown to the CR receiver in practice. This in turn may considerably degrade the performance of the GLR detectors.

To achieve communications and enhance spectrum utilization, the SU needs to reliably detect unoccupied channels within a short sensing period. In such a situation, the stationary samples available for spectrum sensing are usually quite limited. This motivates us to develop efficient approaches that can work in data-limited scenarios, e.g., where the number of samples is comparable with the number of antennas. It should be pointed out that the AGM and GLR algorithms have their root in the maximum likelihood (ML) estimation theory and therefore are asymptotically optimal only in the large-sample-size limit. For relatively small-sample scenarios whereby the number of antennas is comparable to the number of samples in magnitude, however, they suffer from performance degradation to various extents. Therefore, it is of considerable interest to develop efficient algorithms for spectrum sensing in the sample-starving situations. As a locally most powerful test, John's detector [18] has been shown in [19] to be superior to the spherical test (ST) [20] at small samples in the community of multivariate statistics. Note that the ST approach has been used in [15] and analyzed in [21] for spectrum sensing, which in fact is equivalent to the AGM algorithm. Later on, John's detector is heuristically applied to spectrum sensing in [22] and [23]. Recently, its sensing performance is accurately analyzed in [24]. For large numbers of samples and antennas, nevertheless, the calculation of the first and second moments of John's test statistic in [24], which are needed to determine the cumulative distribution function (CDF) of the approximate beta distribution, is computationally intensive. Moreover, note that the CDF varies with the number of antennas m and number of samples n, requiring additional storage and computations. Thus, the overhead renders real-time sensing difficulty. This will be further deliberated in Section IV.

In this paper, an eigenvalue moment ratio (EMR) algorithm is devised for spectrum sensing from the perspective of the random matrix theory (RMT) [25]–[27], i.e., the ratio of the jth moment of the sample eigenvalues calculated from an $m \times n$ signal-free observation matrix to the jth power of the first moment of the sample eigenvalues almost surely (a.s.) converges to a deterministic value as $m, n \to \infty$ with $m/n \to c \in (0, \infty)$. Here, j is an integer larger than or equal to 2. It is worth noting that, although the EMR approach with $j = 2$ offers the same expression as John's detector [18], they are developed from different perspectives because the latter is derived by maximizing the power function. Meanwhile, it should also be pointed out that John's detector is originally developed from the assumption of $n \to \infty$ with m being fixed. In contrast to John's approach, the EMR detector is devised in the regime of $m, n \to \infty$ and $m/n \to c$. Indeed, John's detector turns out to be the simplest case among the EMR schemes with $j \geq 2$ since the former only utilizes the first and second moments of the sample eigenvalues, i.e., $j = 2$. The simulation results in Section IV will also verify that the EMR approach has different behaviors from John's scheme.

In addition to the derivation of the EMR algorithm from the RMT perspective, the contributions of this paper include 1) calculation of the theoretical decision threshold for the EMR method, which turns out to be very accurate for finite numbers of samples and antennas; 2) derivation of the asymptotic distribution of the EMR statistic in the presence of signals, which enables us to correctly analyze the detection performance; and 3) reformulation of the EMR detector in terms of the Frobenius inner product and matrix trace operations, avoiding the eigenvalue decomposition (EVD) of the SCM and thereby saving the computational cost. Note that all signal eigenvalues are exploited in the EMR algorithm, whereas only the largest signal eigenvalue is employed in the rank-1 GLR and MME methods. As a result, the EMR method is superior to the rank-1 GLR and MME detectors in the situation of multiple PUs, particularly under low SNR and relatively small-sample environment.

The remainder of this paper is organized as follows. In Section II, the signal model is described, and conventional spectrum sensing algorithms are reviewed. In Section III, the theoretical threshold of the EMR detector is computed, and its detection probability is derived. Simulation results are provided in Section IV. Finally, conclusions are drawn in Section V.

II. Problem Formulation

A. Signal Model

Consider a multiple-input–multiple-output (MIMO) CR network where the SU has m antennas to receive the signals emitted by $d(d < m)$ PUs with a single antenna. The output of the SU, $\boldsymbol{x}_k(k = 1, \ldots, n)$, under two hypotheses [$\mathcal{H}_0$ (signal absence) and $\mathcal{H}_1$ (signal presence)] can be written as[1]

$$\boldsymbol{x}_k = \begin{cases} \boldsymbol{w}_k, & \mathcal{H}_0 \\ \boldsymbol{H}\boldsymbol{s}_k + \boldsymbol{w}_k, & \mathcal{H}_1 \end{cases} \tag{1}$$

where $\boldsymbol{H} \in \mathbb{C}^{m \times d}$ contains the MIMO channel coefficients between the PUs and SU, which are deterministic unknown during the sensing period, and $\boldsymbol{x}_k = [x_1(k), \ldots, x_m(k)]^T$, $\boldsymbol{s}_k = [s_1(k), \ldots, s_d(k)]^T$, and $\boldsymbol{w}_k = [w_1(k), \ldots, w_m(k)]^T$ stand for the observation, signal, and noise vectors at the kth sampling instant, respectively. Here, $(\cdot)^T$ is the transpose, $x_i(k)(i = 1, \ldots, m)$ stands for the output of the ith antenna, $s_i(k)(i = 1, \ldots, d)$ is the ith primary signal following an i.i.d. complex Gaussian distribution with zero mean and unknown variance $\sigma_{s_i}^2$, and $w_i(k)(i = 1, \ldots, m)$ is the additive noise at the ith antenna, modeled as an i.i.d. complex Gaussian random process with zero mean and unknown variance τ. Furthermore, the noises are assumed uncorrelated with the signals. Since $\boldsymbol{x}_k$ is zero-mean Gaussian distributed, only the covariance matrix is needed to characterize its statistical behavior. The population

[1]For the situation of single-antenna sensing, the oversampled model can be exactly written as (1) but with different structures in the channel matrix $\boldsymbol{H}$ and signals $\boldsymbol{s}_k$, which has been widely discussed in the literature [8], [14]. As a result, this case is not discussed here.

covariance matrix is calculated as $\boldsymbol{R} \triangleq \mathrm{E}[\boldsymbol{x}_k \boldsymbol{x}_k^H]$, which, under the two hypotheses, can be written as

$$\boldsymbol{R} = \begin{cases} \tau \boldsymbol{I}_m, & \mathcal{H}_0 \\ \boldsymbol{H}\boldsymbol{R}_s\boldsymbol{H}^H + \tau \boldsymbol{I}_m, & \mathcal{H}_1 \end{cases} \tag{2}$$

where $(\cdot)^H$ denotes the conjugate transpose, $\boldsymbol{I}_m$ is the $m \times m$ identity matrix, $\boldsymbol{R}_s = \mathrm{E}[\boldsymbol{s}_k \boldsymbol{s}_k^H]$ is the primary signal covariance matrix, and $\mathrm{E}[\cdot]$ is the mathematical expectation.

B. Conventional Sensing Solutions

The popular detector employing signal magnitude information is the energy detector (ED) [5], which is given as

$$\xi_{\mathrm{ED}} \triangleq \frac{\sum_{k=1}^{n} \boldsymbol{x}_k^H \boldsymbol{x}_k}{\tau} \underset{\mathcal{H}_0}{\overset{\mathcal{H}_1}{\gtrless}} \gamma_{\mathrm{ED}} \tag{3}$$

where γ_{ED} is its decision threshold. If $\xi_{\mathrm{ED}} > \gamma_{\mathrm{ED}}$, the signal is present; otherwise, the signal is absent. Given the noise variance, the ED is the optimal detector for i.i.d. observed data [28]. When it is unknown, its estimate $\hat{\tau}$ is used instead. In this case, the performance of the ED usually degrades dramatically since it is quite sensitive to the error in $\hat{\tau}$, which is also known as noise uncertainty [29]. To improve the robustness against the noise uncertainty, the blind detection methods using the signal correlation structure have been developed.

Due to the deterministic channel over the sensing interval and/or correlation among the signal samples, the signal-plus-noise covariance matrix loses the identity structure. Utilizing this nonidentity structure, the CAV scheme [6] is heuristically devised as

$$\xi_{\mathrm{CAV}} \triangleq \frac{\sum_{i=1}^{m}\sum_{j=1}^{m} |\hat{r}_{i,j}|}{\frac{1}{m}\sum_{i=1}^{m} |\hat{r}_{i,i}|} \underset{\mathcal{H}_0}{\overset{\mathcal{H}_1}{\gtrless}} \gamma_{\mathrm{CAV}} \tag{4}$$

where $\hat{r}_{i,j}$ is the (i,j) entry of the SCM $\hat{\boldsymbol{R}} \triangleq (1/n)\sum_{k=1}^{n} \boldsymbol{x}_k \boldsymbol{x}_k^H$, and γ_{CAV} is the threshold of the CAV method.

Indeed, the nonidentity structure of $\boldsymbol{R}$ leads to the significant spread out of eigenspectrum, providing a good indication for the primary signals. Consequently, the eigenvalues have been employed in numerous approaches for spectrum sensing, such as the AGM [13], [15], [16], and GLR [9], [17], [30], all of which are derived in the framework of the GLR test. A variant of the AGM detector is given by [31]

$$\xi_{\mathrm{AGM}} \triangleq 2(n-1)\log\left(\frac{\frac{1}{m}\sum_{i=1}^{m}\ell_i}{\left(\prod_{i=1}^{m}\ell_i\right)^{\frac{1}{m}}}\right)^{m} \underset{\mathcal{H}_0}{\overset{\mathcal{H}_1}{\gtrless}} \gamma_{\mathrm{AGM}} \tag{5}$$

where $\ell_1 \geq \cdots \geq \ell_m$ are the decreasing sample eigenvalues of $\hat{\boldsymbol{R}}$ and γ_{AGM} is the decision threshold of the AGM approach. If the number of PUs (or rank) is *a priori* known, accurate variants of the GLR approach are devised in [9], [10], [17], and [30]. In the presence of a single PU, the rank-1 GLR detector [9] employs the scaled largest eigenvalue (SLE) [9], [10], [30] as its test statistic, which is also called the SLE detector and is expressed as

$$\xi_{\mathrm{SLE}} \triangleq \frac{\ell_1}{1/m\sum_{i=1}^{m}\ell_i} \underset{\mathcal{H}_0}{\overset{\mathcal{H}_1}{\gtrless}} \gamma_{\mathrm{SLE}} \tag{6}$$

where γ_{SLE} is the decision threshold of the SLE approach. In the presence of d primary signals with $1 < d < m$, nevertheless, the rank-d GLR scheme [17] has a more complicated form, i.e.,

$$\xi_{\mathrm{GLR}} \triangleq \frac{1/m\sum_{i=1}^{m}\ell_i}{\left(\prod_{i=1}^{m}\ell_i\right)^{1/m}} \Bigg/ \frac{1/(m-d)\sum_{i=d+1}^{m}\ell_i}{\left(\prod_{i=d+1}^{m}\ell_i\right)^{1/(m-d)}} \underset{\mathcal{H}_0}{\overset{\mathcal{H}_1}{\gtrless}} \gamma_{\mathrm{GLR}} \tag{7}$$

where γ_{GLR} is the threshold of the GLR algorithm. As another single-source detector, the MME detector [8] exploits the condition number as the test statistics

$$\xi_{\mathrm{MME}} \triangleq \frac{\ell_1}{\ell_m} \underset{\mathcal{H}_0}{\overset{\mathcal{H}_1}{\gtrless}} \gamma_{\mathrm{MME}} \tag{8}$$

where γ_{MME} is the decision threshold. Nevertheless, it is hard to justify the assumption that the number of primary signals is *a priori* known to the receiver in practice. As a result, the SLE, rank-d GLR, and MME suffer from performance degradation when d is unknown and changes in different situations.

The decision threshold γ can be determined by solving $F(\gamma) = 1 - P_{\mathrm{fa}}$, where P_{fa} denotes the false-alarm probability and $F(x)$ is the CDF of the statistic under $\mathcal{H}_0$. The CDF can be determined via theoretical derivation or Monte Carlo simulation. The analytical threshold expressions of various detectors for $P_{\mathrm{fa}} = \varepsilon$ and complex-valued observations are tabulated in Table I. The threshold formulas in the second column are derived from the asymptotic distribution of the test statistic. Specifically, the thresholds of the SLE and MME are derived in the regime where $m, n \to \infty$ and $m/n \to c$, whereas those of the CAV and AGM are computed in the regime of fixed m and $n \to \infty$. These thresholds are asymptotically optimal but suffer from an error for finite numbers of antennas and samples.

The exact analytical CDF formulas have been developed for the SLE and MME statistics in [11], [32], and [33], allowing us to obtain the exact thresholds for finite numbers of antennas and samples, as shown in the third column of Table I. However, their evaluation is much more computationally intensive than the calculation of the asymptotic thresholds. Moreover, the dynamic range (DR) of the summands of the analytical CDF expression is so high particularly for large numbers of antennas and samples that extremely high numerical precision and wide range of values are required for accurate evaluation of the CDF expression without numeric overflow.

To find the decision threshold by the Monte Carlo simulation, we vary the threshold within a certain range, and for each threshold value, we repeatedly perform binary decision on a large number of random Gaussian noise realizations. A P_{fa} curve as a function of decision threshold is thus obtained. From this curve, the threshold is then identified as the one that corresponds to a desired P_{fa}.

III. Eigenvalue-Moment-Ratio Detector and Performance Analysis

Here, we first derive the blind EMR algorithm from the RMT perspective, in which the channels, primary signal number, signal power, and noise power are all unknown. Then, we

TABLE I
FORMULA FOR THEORETICAL THRESHOLD COMPUTATION WITH COMPLEX-VALUED OBSERVATIONS

Method	Theoretical threshold (γ)	
	Asymptotic	Exact
scaled largest eigenvalue (SLE)	$\left(1+\sqrt{\frac{m+1/2}{n+1/2}}\right)^2 + \frac{(\sqrt{m+1/2}+\sqrt{n+1/2})^{4/3}}{n[(m+1/2)(n+1/2)]^{1/6}} F_2^{-1}(1-\varepsilon)$ *a [9], [30]	$\bar{F}_{\text{SLE}}^{-1}(\varepsilon)$ *b
maximum-minimum eigenvalue (MME)	$\frac{(\sqrt{n+1/2}+\sqrt{m+1/2})^2}{(\sqrt{n+1/2}-\sqrt{m+1/2})^2} \times \left(1+\frac{(\sqrt{n+1/2}+\sqrt{m+1/2})^{-2/3}}{[(m+1/2)(n+1/2)]^{1/6}} F_2^{-1}(1-\varepsilon)\right)$ *a [8], [30]	$1/(1-\bar{F}_Y^{-1}(\varepsilon))$ *c
arithmetic-to-geometric mean (AGM)	$2/c_1\bar{\Gamma}^{-1}(1-\varepsilon, m^2-1)$ *d [31]	N/A
covariance absolute value (CAV)	$\frac{1+(m-1)\sqrt{2/(n\pi)}}{1-Q^{-1}(\varepsilon)\sqrt{2/n}}$ [6]	N/A
energy detector with known τ (ED(τ))	N/A	$2\bar{\Gamma}^{-1}(1-\varepsilon, 2mn)$ *d [31]
energy detector with estimated τ (ED($\hat{\tau}$))	$c_2(1+c_3Q^{-1}(\varepsilon))$ *d [31]	N/A

*a $F_2(\cdot)$ is the CDF of the Tracy-Widom distribution of order two [34].
*b $\bar{F}_{\text{SLE}}$ is the complementary CDF (tail distribution) of the SLE defined in [32, (14)] or [33, Theorem 1].
*c $\bar{F}_Y$ is defined in [11, Theorem 1].
*d $c_1 = 1-(2m^2+1)/(6mn)$, $c_2 = L/(L-1)$ and $c_3 = \sqrt{(mn+L-1)/(mn(L-2))}$ are the correction factors [31]. $\bar{\Gamma}^{-1}(\cdot)$ is the inverse of the incomplete gamma function.

analyze its performance in terms of detection probability P_d and false-alarm probability P_{fa}. Since both P_d and P_{fa} vary with the threshold, a common practice is to evaluate P_d for a fixed P_{fa}. Employing the existing RMT results, the theoretical threshold of the EMR approach is determined. To compute P_d, we need the distribution of ξ_{EMR} under $\mathcal{H}_1$, which, however, is unavailable in the literature. To address this, we derive the asymptotic distribution of ξ_{EMR} under $\mathcal{H}_1$ based on the RMT [35] and then use it to obtain an approximate analytical formula for the detection probability.

A. EMR Algorithm

To derive the EMR statistic, we need the following results.

Proposition 1: Let $\hat{\boldsymbol{R}}$ be the SCM of the signal-free observation matrix $\boldsymbol{X} = [\boldsymbol{x}_1, \ldots, \boldsymbol{x}_n] \in \mathbb{C}^{m\times n}$ whose elements are i.i.d. Gaussian variables with zero mean and variance τ. Then, the ratio of the jth moment of the sample eigenvalues $\{\ell_i\}_{i=1}^m$, denoted by $\hat{\mathcal{M}}_j$, to the jth power of the first moment of ℓ_i a.s. converges to a constant independent of τ as $m, n \to \infty$ and $m/n \to c \in (0, \infty)$, i.e.,

$$\xi_{\text{EMR}}^{(j)} \triangleq \frac{\hat{\mathcal{M}}_j}{(\hat{\mathcal{M}}_1)^j} = \frac{\frac{1}{m}\sum_{i=1}^m \ell_i^j}{\left(\frac{1}{m}\sum_{i=1}^m \ell_i\right)^j} \xrightarrow{\text{a.s.}} \eta(j) \tag{9}$$

where $\eta(j) = \sum_{k=0}^{j-1}(c^k/(k+1))C_j^k C_{j-1}^k$, and C_j^k denotes the total number of k-combinations of j numbers.

Proof: It is shown in [26] and [27] that $\hat{\mathcal{M}}_j$ a.s. converges to the jth moment of the population eigenvalues associated with $\boldsymbol{R}$ as $m, n \to \infty$ and $m/n \to c$, i.e.,

$$\hat{\mathcal{M}}_j \xrightarrow{\text{a.s.}} \mathcal{M}_j \triangleq \int t^j dF^{\boldsymbol{R}}(t). \tag{10}$$

Note that this result was first verified in [36], later on proved in [26] by using a method of moment, and well summarized in [27]. Here, $dF^{\boldsymbol{R}}(t)$ is the Marčenko–Pastur density, and $\mathcal{M}_j$ is calculated as

$$\mathcal{M}_j = \tau^j \sum_{k=0}^{j-1} \frac{c^k}{k+1} C_j^k C_{j-1}^k \triangleq \tau^j \eta(j). \tag{11}$$

As a result, substituting $\hat{\mathcal{M}}_j = (1/m)\sum_{i=1}^m \ell_i^j$ along with (11) into (10), we obtain

$$\left(\frac{1}{m}\sum_{i=1}^m \ell_i\right)^j \xrightarrow{\text{a.s.}} \tau^j \tag{12a}$$

$$\frac{1}{m}\sum_{i=1}^m \ell_i^j \xrightarrow{\text{a.s.}} \tau^j \eta(j) \tag{12b}$$

whose ratio leads to the proof of Proposition 1. ■

It is indicated in Proposition 1 that, as $m, n \to \infty$ and $m/n \to c$, the EMR statistic, i.e., $\xi_{\text{EMR}}^{(j)}(j \geq 2)$, a.s. converges to a constant independent of the noise variance. The simplest case among them is $j = 2$, i.e.,

$$\xi_{\text{EMR}}^{(2)} = \frac{\hat{\mathcal{M}}_2}{(\hat{\mathcal{M}}_1)^2} = \frac{\frac{1}{m}\sum_{i=1}^m \ell_i^2}{\left(\frac{1}{m}\sum_{i=1}^m \ell_i\right)^2} \xrightarrow{\text{a.s.}} 1 + c. \tag{13}$$

Obviously, the presence of primary signals violates the limiting behavior of $\xi_{\text{EMR}}^{(2)}$, thereby providing a good indication for the primary signals.

Recall that

$$\hat{\mathcal{M}}_1 = \frac{1}{m}\sum_{i=1}^m \ell_i = \frac{1}{m}\text{tr}(\hat{\boldsymbol{R}}) \tag{14}$$

where $\text{tr}(\cdot)$ denotes the matrix trace, and

$$\hat{\mathcal{M}}_2 = \frac{1}{m}\sum_{i=1}^m \ell_i^2 = \frac{1}{m}\text{tr}(\hat{\boldsymbol{R}}\hat{\boldsymbol{R}}^H). \tag{15}$$

On the other hand, notice that

$$\text{tr}(\hat{\boldsymbol{R}}\hat{\boldsymbol{R}}^H) = \sum_{i=1}^m \sum_{j=1}^m |\hat{r}_{i,j}|^2 = \|\hat{\boldsymbol{R}}\|_F^2 \tag{16}$$

TABLE II
EMR DETECTION ALGORITHM

Step 1: Compute the SCM by $\hat{\boldsymbol{R}} = (1/n)\sum_{k=1}^{n} \boldsymbol{x}_k \boldsymbol{x}_k^{\mathrm{H}}$.
Step 2: Calculate the first and second moments of the sample eigenvalues via

$$\hat{\mathcal{M}}_1 = \frac{1}{m}\,\mathrm{tr}(\hat{\boldsymbol{R}}), \quad \hat{\mathcal{M}}_2 = \frac{1}{m}\left\|\hat{\boldsymbol{R}}\right\|_{\mathrm{F}}^2.$$

Step 3: Determine the presence of the primary signals by comparing $\xi_{\mathrm{EMR}} = \hat{\mathcal{M}}_2/\left(\hat{\mathcal{M}}_1\right)^2$ with the predetermined threshold γ_{EMR}. If $\xi_{\mathrm{EMR}} > \gamma_{\mathrm{EMR}}$, the signal is present; otherwise, the signal does not exist.

TABLE III
NUMBER OF FLOPS REQUIRED IN EMR AND STATE-OF-THE-ART DETECTORS

Method	Calculation of $\hat{\boldsymbol{R}}$	EVD of $\hat{\boldsymbol{R}}$	Norm of $\hat{\boldsymbol{R}}$	Total
SLE MME AGM	m^2n	$\mathcal{O}(m^3)$	$--$	$m^2n + \mathcal{O}\left(m^3\right)$
ED(τ)	$--$	$--$	mn	mn
CAV EMR	m^2n	$--$	m^2	$m^2(n+1)$

where $\|\cdot\|_F$ denotes the Frobenius norm. Thus, the EMR decision rule can be expressed as

$$\xi_{\mathrm{EMR}} \triangleq \frac{\hat{\mathcal{M}}_2}{(\hat{\mathcal{M}}_1)^2} = \frac{\frac{1}{m}\|\hat{\boldsymbol{R}}\|_F^2}{\left(\frac{1}{m}\mathrm{tr}(\hat{\boldsymbol{R}})\right)^2} \underset{\mathcal{H}_0}{\overset{\mathcal{H}_1}{\gtrless}} \gamma_{\mathrm{EMR}} \tag{17}$$

where γ_{EMR} is the threshold of the EMR method, which will be determined using the asymptotic distribution of ξ_{EMR} under $\mathcal{H}_0$ in the following. The proposed EMR method for spectrum sensing is summarized in Table II.

Note that, unlike the existing eigenvalue-based methods, the EMR detector does not rely on the EVD of $\hat{\boldsymbol{R}}$ to calculate the test statistic. Instead, it uses the Frobenius norm and the trace of $\hat{\boldsymbol{R}}$, which is similar to the CAV detector. As the EVD of $\hat{\boldsymbol{R}}$ requires $\mathcal{O}(m^3)$ floating-point operations (flops), whereas the Frobenius norm and trace of $\hat{\boldsymbol{R}}$ only involve m^2 flops, the EMR detector is more computationally efficient than the eigenvalue-based methods [7]–[13], [15], [31]. The computational complexity of the EMR and those of the other methods are summarized in Table III.

Remark 1: As should be pointed out, the EMR $\xi_{\mathrm{EMR}}^{(j)}$ for $j > 2$ can also be exploited for spectrum sensing, and its behavior will be numerically investigated in Section IV. Nevertheless, since it relies on the jth moment of the sample eigenvalues whose asymptotic fluctuation is very difficult to determine, its performance cannot yet be theoretically analyzed. This will be addressed in our future work. On the other hand, note that, for $j = 2$, the EMR algorithm is reduced to John's method, although the former is devised from the RMT perspective in the regime where $m, n \to \infty$ and $m/n \to c$, whereas the latter is developed from the perspective of maximizing the power function in the situation where $n \to \infty$ and m is fixed. Thus, the EMR detector is different from John's approach in the derivation regimes and perspectives.

B. Theoretical Decision Threshold

To obtain the constant false-alarm rate property, we need to find a threshold for decision reference, which must be deterministic and independent of τ. Such a theoretical threshold is determined here. The asymptotical fluctuation of ξ_{EMR} under $\mathcal{H}_0$ is described by the following lemma.

Lemma 1: Assume $\hat{\boldsymbol{R}}$ satisfies the hypotheses of Proposition 1. The statistic

$$\zeta \triangleq m\left[\xi_{\mathrm{EMR}} - (1+c)\right] \tag{18}$$

converges in distribution to a Gaussian process with mean zero and variance $2c^2$ as $m, n \to \infty$, $m/n \to c \in (0, \infty)$, i.e.,

$$\zeta \xrightarrow{\mathcal{D}} \mathcal{N}(0, 2c^2) \tag{19}$$

where $\xrightarrow{\mathcal{D}}$ denotes the convergence in distribution, and $\mathcal{N}(0, \sigma^2)$ is the real Gaussian distribution with zero mean and variance σ^2.

Proof: Based on the joint distribution of $\hat{\mathcal{M}}_1$ and $\hat{\mathcal{M}}_2$ in [26] for the real case and in [37] for the complex situation, (19) is proved in [27] using the Delta method [38]. ■

The false-alarm probability for the EMR is calculated as

$$\begin{aligned} P_{\mathrm{fa}} &= P(\xi_{\mathrm{EMR}} > \gamma_{\mathrm{EMR}} | \mathcal{H}_0) \\ &= P\left(\frac{m\left[\xi_{\mathrm{EMR}} - (1+c)\right]}{\sqrt{2}c} > \frac{m\left[\gamma_{\mathrm{EMR}} - (1+c)\right]}{\sqrt{2}c}\,\middle|\,\mathcal{H}_0\right) \\ &= \int_{\frac{m[\gamma_{\mathrm{EMR}}-(1+c)]}{\sqrt{2}c}}^{\infty} \frac{1}{\sqrt{2\pi}} \exp\left(-\frac{1}{2}t^2\right) dt \\ &= Q\left(\frac{m\left[\gamma_{\mathrm{EMR}} - (1+c)\right]}{\sqrt{2}c}\right) \end{aligned} \tag{20}$$

where

$$Q(x) = \frac{1}{\sqrt{2\pi}} \int_x^{\infty} \exp\left(-\frac{t^2}{2}\right) dt. \tag{21}$$

For a desired false-alarm rate ε, the associated threshold should be chosen such that

$$\gamma_{\mathrm{EMR}} = 1 + c + \frac{\sqrt{2}cQ^{-1}(\varepsilon)}{m}. \tag{22}$$

The relative errors (REs) between the asymptotically derived and simulated thresholds are plotted in Fig. 1 for the EMR and other algorithms. Here, n varies from 5 up to 150 with $m/n = 0.8$ and $P_{\mathrm{fa}} = 0.01$. The RE is defined as $|\gamma_{\mathrm{the}} - \gamma_{\mathrm{sim}}|/\gamma_{\mathrm{sim}} \times 100\%$ with γ_{the} and γ_{sim} being the theoretical and simulated thresholds, respectively. The simulated thresholds are obtained using 10^6 Monte Carlo trials. In the ED($\hat{\tau}$), $L = n$ signal-free samples are assumed available to estimate the noise variance.

Fig. 1 implies that the CAV has the largest error in threshold prediction. This is because its theoretical threshold is determined in the framework of the central limit theorem (CLT), according to which, the entries of the noise-only SCM are approximately Gaussian distributed when the sample size is

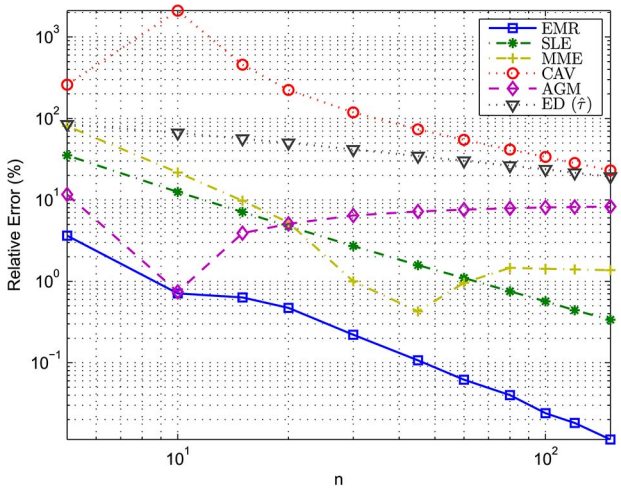

Fig. 1. Relative error of asymptotic theoretical threshold versus number of samples for various methods. $m/n = 0.08$, and $P_{\rm fa} = 0.01$.

sufficiently large [6].[2] For small-sample scenarios, the theoretical threshold is not accurate. For the ED($\hat{\tau}$), accurate threshold prediction relies on the condition that sufficient independent noise-only samples are available for noise variance estimation, whereby the estimated noise variance is approximated by Gaussian distribution [31]. Although the error of theoretical threshold of the AGM is relatively small, it increases with m or n when $n \geq 10$. This is due to the fact that, similar to the CAV detector, its theoretical threshold is also determined in the fixed m large n limit. In contrast, the threshold formulas for the EMR/SLE/MME are derived based on the large m relatively large n asymptotics, and their errors are thereby relatively small and gradually decrease with m or n. Note that the MME carries much larger error in threshold prediction than the EMR and SLE. It is because, in the theoretical threshold computation, the minimum eigenvalue in the denominator of the MME statistic is replaced by its limiting value $\tau(1-\sqrt{c})^2$, and its fluctuation is ignored. This can lead to a large error particularly when c approaches 1. Similarly, the fluctuation of the summation of the noise eigenvalues is also ignored in [9] for the threshold calculation, incurring a large error for the SLE. Unlike the MME and SLE, the EMR does not ignore any fluctuation in its theoretical threshold computation, thereby providing the smallest threshold prediction error. It is equal to 3.64% for $n = 5$ and 0.71% for $n = 10$ and drops below 0.1% when $n > 45$. This implies that the asymptotic fluctuation of the EMR statistic provides a good approximation for finite m and n. In Table IV, we fix $m = 12$ and $n = 15$, and vary $P_{\rm fa}$ from 10^{-4} up to 0.1. It is seen that the REs of the EMR are below 4% and consistently less than those of all other detectors.

Remark 2: One potential advantage of the EMR test is that it might be able to better match the false-alarm specifications imposed in modern communication systems. For example, with regard to the required sensing sensitivity according to the IEEE 802.22 standard [4], [39], the SNR is as low as -21 dB for digital TV signal and -12 dB for wireless microphone signal, whereas the false-alarm probability must be not over 0.1. The EMR test enjoys the advantage of better matching such a false-alarm requirement.

[2]Note that, although the CAV detector is generally applicable for both large- and small-sample scenarios, its theoretical threshold [6] is derived based on the CLT and is only accurate for large-sample scenarios but not accurate for small-sample situations.

TABLE IV
RELATIVE ERROR OF ASYMPTOTIC THEORETICAL THRESHOLD FOR VARIOUS METHODS. $m = 12$, AND $n = 15$

Detector	EMR	SLE	MME	CAV	AGM	ED($\hat{\tau}$)	$P_{\rm fa}$
Theo γ	2.15	4.43	423.20	-9.12	293.00	2.22	10^{-4}
Empi γ	2.23	4.02	1195.3	4.16	309.63	10.80	
RE (%)	3.60	10.19	64.59	319.08	5.37	79.45	
Theo γ	2.09	4.13	395.97	-25.44	274.44	2.02	10^{-3}
Empi γ	2.14	3.81	635.72	4.04	286.86	6.95	
RE (%)	2.05	8.60	37.71	729.49	4.33	70.85	
Theo γ	2.02	3.80	364.51	21.70	252.94	1.79	10^{-2}
Empi γ	2.03	3.55	332.53	3.89	263.00	4.11	
RE (%)	0.62	7.07	9.62	458.25	3.83	56.50	
Theo γ	1.92	3.36	324.03	6.14	225.36	1.47	10^{-1}
Empi γ	1.91	3.23	158.98	3.70	232.06	2.14	
RE (%)	0.55	3.98	103.82	65.90	2.89	31.48	

C. Detection Probability

To predict the detection probability, we need to know the distribution of $\xi_{\rm EMR}$ under $\mathcal{H}_1$. To this end, we derive an approximate analytical expression for the distribution of $\xi_{\rm EMR}$ based on the RMT [35]. First, we have the following proposition for the distribution of $\xi_{\rm EMR}$ in the presence of d "asymptotically identifiable" signals whose population eigenvalues are above the asymptotic limit of detection.

Proposition 2: Denote the signal population eigenvalues of

$$\boldsymbol{\Psi} = \boldsymbol{H}\boldsymbol{R}_s\boldsymbol{H}^H \tag{23}$$

by $\lambda_1 \geq \lambda_2 \geq \cdots \geq \lambda_d > 0$. Assume

$$\lambda_d > \lambda_{\rm DET} \triangleq \sqrt{c}\tau \tag{24}$$

where $\lambda_{\rm DET}$ is the asymptotic limit of detection. As $m, n \to \infty$ and $m/n \to c \in (0, \infty)$, we have

$$\xi_{\rm EMR} \xrightarrow{\mathcal{D}} \mathcal{N}\left(\mu_\xi, \sigma_\xi^2\right) \tag{25}$$

where

$$\mu_\xi = \frac{m\left[\nu_2 + (m-d)\tau^2(1+c)\right]}{\left[\nu_1 + (m-d)\tau\right]^2} \tag{26}$$

$$\sigma_\xi^2 = \boldsymbol{\nabla}^T\boldsymbol{D}\boldsymbol{\nabla} \tag{27}$$

with

$$\nu_1 = \sum_{i=1}^{d}(\lambda_i + \tau)\left(1 + \frac{c\tau}{\lambda_i}\right) \tag{28a}$$

$$\nu_2 = \sum_{i=1}^{d}(\lambda_i + \tau)^2\left(1 + \frac{c\tau}{\lambda_i}\right)^2 \tag{28b}$$

$$\boldsymbol{D} = \tau^2 c\begin{bmatrix} 1 & 2\tau(1+c) \\ 2\tau(1+c) & 2\tau^2(2c^2+5c+2) \end{bmatrix} \tag{29a}$$

$$\boldsymbol{\nabla} = \frac{m}{\left[\nu_1 + (m-d)\tau\right]^3}\begin{bmatrix} -1\left[\nu_2 + (m-d)\tau^2(1+c)\right] \\ \nu_1 + (m-d)\tau \end{bmatrix}. \tag{29b}$$

Proof: The proof of Proposition 2 is provided in Appendix A. ■

According to Proposition 2, the detection probability is

$$\begin{aligned} P_d &= P(\xi_{\mathrm{EMR}} > \gamma_{\mathrm{EMR}} | \mathcal{H}_1) \\ &= P\left(\frac{\xi_{\mathrm{EMR}} - \mu_\xi}{\sigma_\xi} > \frac{\gamma_{\mathrm{EMR}} - \mu_\xi}{\sigma_\xi} \middle| \mathcal{H}_1 \right) \\ &= Q\left(\frac{\gamma_{\mathrm{EMR}} - \mu_\xi}{\sigma_\xi} \right) \end{aligned} \tag{30}$$

where μ_ξ and σ_ξ^2 are given by (26) and (27), respectively.

In Proposition 2, we assume that all the d signals are identifiable in the sense that their population eigenvalues are above λ_{DET}. In what follows, we consider a mixture of q $(q < d)$ identifiable signals whose signal eigenvalues are greater than λ_{DET} and $(d-q)$ unidentifiable signals whose signal eigenvalues are less than or equal to λ_{DET}.

Proposition 3: Assume the ordered signal population eigenvalues satisfy

$$\lambda_1 \geq \cdots \geq \lambda_q > \lambda_{\mathrm{DET}} > \lambda_{q+1} \geq \cdots \geq \lambda_d. \tag{31}$$

As $m, n \to \infty$ and $m/n \to c \in (0, \infty)$, we have

$$\xi_{\mathrm{EMR}} \xrightarrow{\mathcal{D}} \mathcal{N}\left(\widetilde{\mu}_\xi, \widetilde{\sigma}_\xi^2\right) \tag{32}$$

where

$$\widetilde{\mu}_\xi = \frac{m\left(\widetilde{\nu}_2 + (m-q)\tau^2(1+c)\right)}{\left(\widetilde{\nu}_1 + (m-q)\tau\right)^2} \tag{33}$$

$$\widetilde{\sigma}_\xi^2 = \widetilde{\boldsymbol{\nabla}}^T \boldsymbol{D} \widetilde{\boldsymbol{\nabla}} \tag{34}$$

with

$$\widetilde{\boldsymbol{\nabla}} = \frac{m}{\left[\widetilde{\nu}_1 + (m-q)\tau\right]^3} \begin{bmatrix} -2\left[\widetilde{\nu}_2 + (m-q)\tau^2(1+c)\right] \\ \widetilde{\nu}_1 + (m-q)\tau \end{bmatrix} \tag{35a}$$

$$\widetilde{\nu}_1 = \sum_{i=1}^{q} (\lambda_i + \tau)\left(1 + \frac{c\tau}{\lambda_i}\right) + \sum_{i=q+1}^{d} \lambda_i \tag{35b}$$

$$\widetilde{\nu}_2 = \sum_{i=1}^{q} (\lambda_i + \tau)^2 \left(1 + \frac{c\tau}{\lambda_i}\right)^2 + \sum_{i=q+1}^{d} \left(\lambda_i^2 + 2\tau\lambda_i\right). \tag{35c}$$

Proof: The proof is given in Appendix B. ■

Consequently, for $\lambda_1 \geq \cdots \geq \lambda_q > \lambda_{\mathrm{DET}} > \lambda_{q+1} \geq \cdots \geq \lambda_d$ and as $m, n \to \infty$ with $m/n \to c$, the detection probability can be computed as (30) by replacing μ_ξ and σ_ξ with $\widetilde{\mu}_\xi$ and $\widetilde{\sigma}_\xi$, respectively.

IV. Simulation Results

A. Detection Performance

Here, we present simulation results to evaluate the performance of the EMR detector. Each result represents an average of 20000 independent Monte Carlo trials. At each run, the channel coefficients of $\boldsymbol{H}$ are randomly generated from a zero-mean circularly symmetric complex Gaussian (ZMCSCG) distribution and then fixed during the sensing time. Moreover, the column vectors of $\boldsymbol{H}$ are normalized to unit norm so that the SNR is defined as $(1/d)\sum_{i=1}^{d} \sigma_{s_i}^2/\tau$. For the purpose of comparison, the simulation results of the detectors shown in Table I are presented as well. Nevertheless, since the MME is inferior to the SLE in detecting a single source [12] (as well as in detecting multiple sources according to our simulations), its simulation results are not included for clarity. The ED is also excluded due to its sensitivity to noise uncertainty [29], [40]. For fair comparison, the simulated decision thresholds of the algorithms are used in signal detection.

First, we consider a CR network where each PU employs a single antenna and carries equal-power and independent data stream. A CR array of $m = 7$ antennas is employed to detect the primary signals using $n = 8$ collected samples at each antenna. The detection probability versus SNR for various numbers of PUs at $P_{\mathrm{fa}} = 10^{-2}$ is shown in Fig. 2. It is shown in Fig. 2(a) that, in the presence of a single primary signal, the SLE has the best performance among all blind detectors. Moreover, the EMR performs almost the same as the SLE. Recall that the AGM algorithm is derived in the framework of the GLR test, which depends on the ML estimate. Although it is optimal in the small-antenna and large-sample limit, for large-antenna and large-sample limit, its optimality cannot be guaranteed. Instead, the EMR is more efficient for relatively small-sample scenarios.

In the situations of more than one primary signals, the EMR outperforms the SLE, and the improvement is more significant with the increase in the primary signal number, as shown in Fig. 2(b)–(d). This is because the former is able to utilize all the signal eigenvalues for signal detection, whereas the latter only exploits the largest signal eigenvalue. The rank-d GLR [17], which relies on the signal number information, does not suffer the performance loss and performs comparably to or even better than the EMR, particularly for medium SNRs in which the signal power values are in the middle or upper half of $[0, \lambda_{\mathrm{DET}})$ [41]. When the numbers of antennas and samples are increased to $m = 12$ and $n = 15$, however, the rank-d GLR is inferior to the EMR, as shown in Fig. 3. Indeed, similar to the AGM, the rank-d GLR is also developed in the framework of GLR test using the ML estimate. Consequently, its optimality is attained in the fixed m large n limit but cannot be guaranteed for the sample-starving case when m is comparable in magnitude with n. On the contrary, the EMR is developed from the RMT perspective in which the numbers of antennas and samples are comparable. Moreover, all the signal eigenvalues have been used for signal detection in the EMR. Thus, the EMR surpasses other detectors, particularly when m is comparable to n and $d \geq 2$.

Next, we examine the effect of the spread out of eigenspectrum, namely, the disparity of the eigenvalues of $\boldsymbol{H}\boldsymbol{R}_s\boldsymbol{H}^H$, on the detection performance. Under the i.i.d. assumption of the channel coefficients, two factors can affect the spread out of eigenspectrum, i.e., the DR of the signal power values and signal correlation. Fig. 4(a) shows the detection probability versus the DR of the signal power values, which is defined as $10\log_{10}(\sigma_{s_2}^2/\sigma_{s_1}^2)$ in decibels. Here, we consider two PUs and assume that their signals are uncorrelated with an average SNR of 7.5 dB. It is observed that, with the increase in the DR, all blind detectors improve in performance, among which

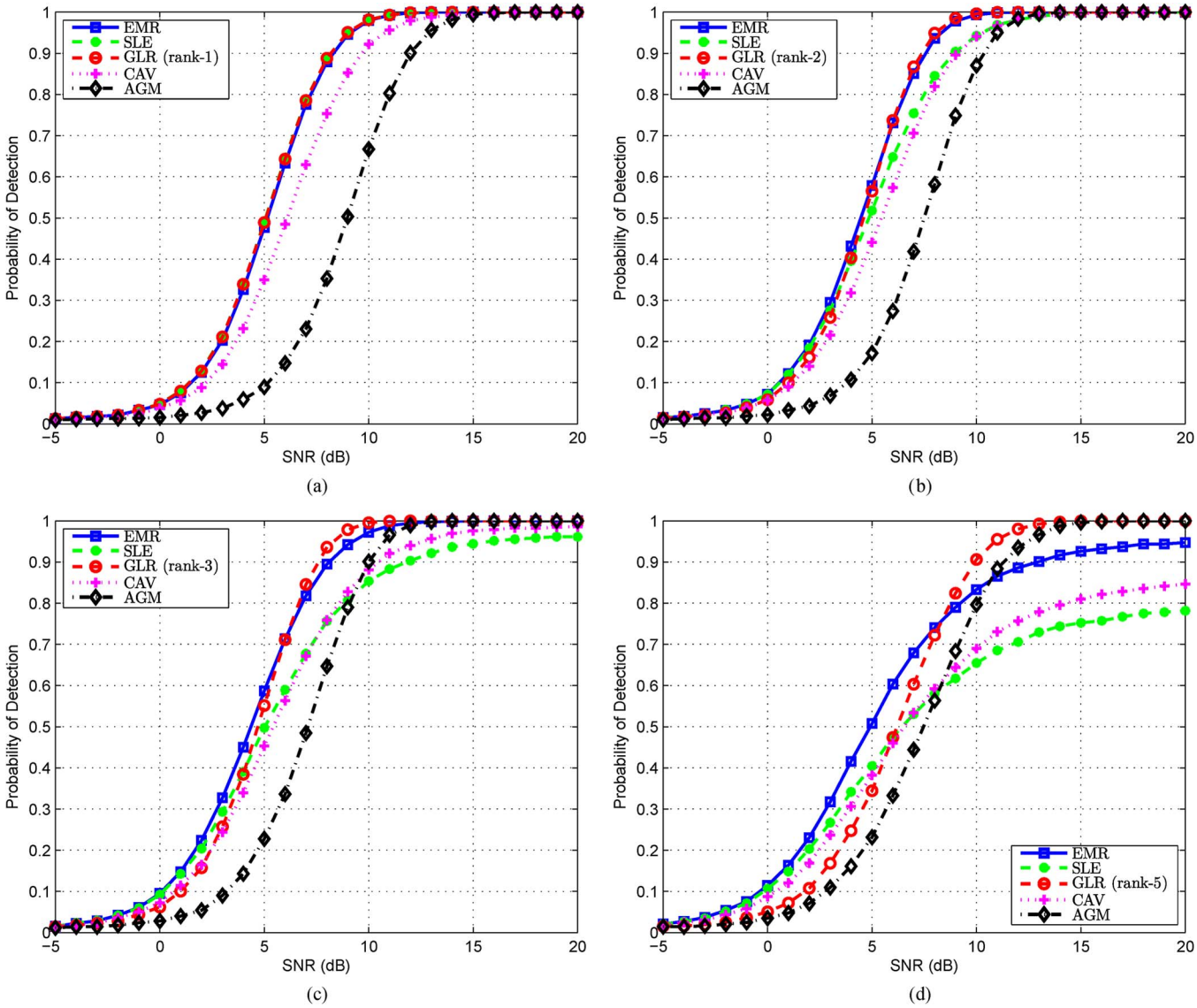

Fig. 2. Probability of detection versus SNR for uncorrelated equal-power primary signals. $m = 7$, $n = 8$, and $P_{\rm fa} = 10^{-2}$. (a) $d = 1$. (b) $d = 2$. (c) $d = 3$. (d) $d = 5$.

the improvement in the SLE detector is the most significant, whereas the enhancement in the rank-2 GLR detector is the least significant. Consequently, when the two signals have close-to-equal power, the rank-2 GLR slightly outperforms the EMR, as indicated in Fig. 2(b) at SNR $= 7.5$ dB. However, as the difference of their power increases, the performance advantage of the former diminishes, and when the DR of the signal power values is larger than 3 dB, it is inferior to the EMR. Likewise, although initially the EMR is superior to the SLE, the performance gap decreases as the power DR widens until it becomes unnoticeable. Fig. 4(b) shows the detection probability versus signal correlation, where the parameters are the same as those in Fig. 2(d) with SNR $= 10$ dB. The correlated signal samples are generated from a first-order autoregressive process as $s_i(k) = \rho s_{i-1}(k) + \sqrt{1-|\rho|^2} \cdot e_i(k), i = 1, \ldots, d$, $k = 1, \ldots, n$, where $e_i(k)$ is the i.i.d. ZMCSCG noise with variance σ_s^2, and ρ is the correlation coefficient (CC). It is observed that the signal correlation has similar effect on the detection performance as the DR of the signal power values. With the increase in the signal correlation, all detectors achieve an improvement by various degrees: the SLE grows fastest, followed by the EMR and CAV, and the rank-5 GLR and AGM grow slowest. As a result, the initial advantage of rank-5 GLR over the EMR, as shown in Fig. 2(d) at SNR $= 10$ dB, diminishes until it becomes negative for increasing signal correlation. This is because, for strongly correlated signals, the energy of multiple signals gradually concentrates on the largest eigenvalue, in which sense multiple signals essentially merge into one signal.

In Fig. 5, the signal power values are assumed to be different, and in each Monte Carlo run, their ratio randomly varies according to a Chi-squared distribution. The empirical receiver operating characteristic (ROC) curves of the EMR are plotted in Fig. 5(a) and (b), where the parameters are the same as those in Figs. 2(c) and 3(b), with the SNR being fixed at 8 and 5 dB, respectively. We see that, under such an unequal-signal-power condition, the EMR consistently performs better or as good as the rank-d GLR and other methods, regardless of $P_{\rm fa}$. Note that

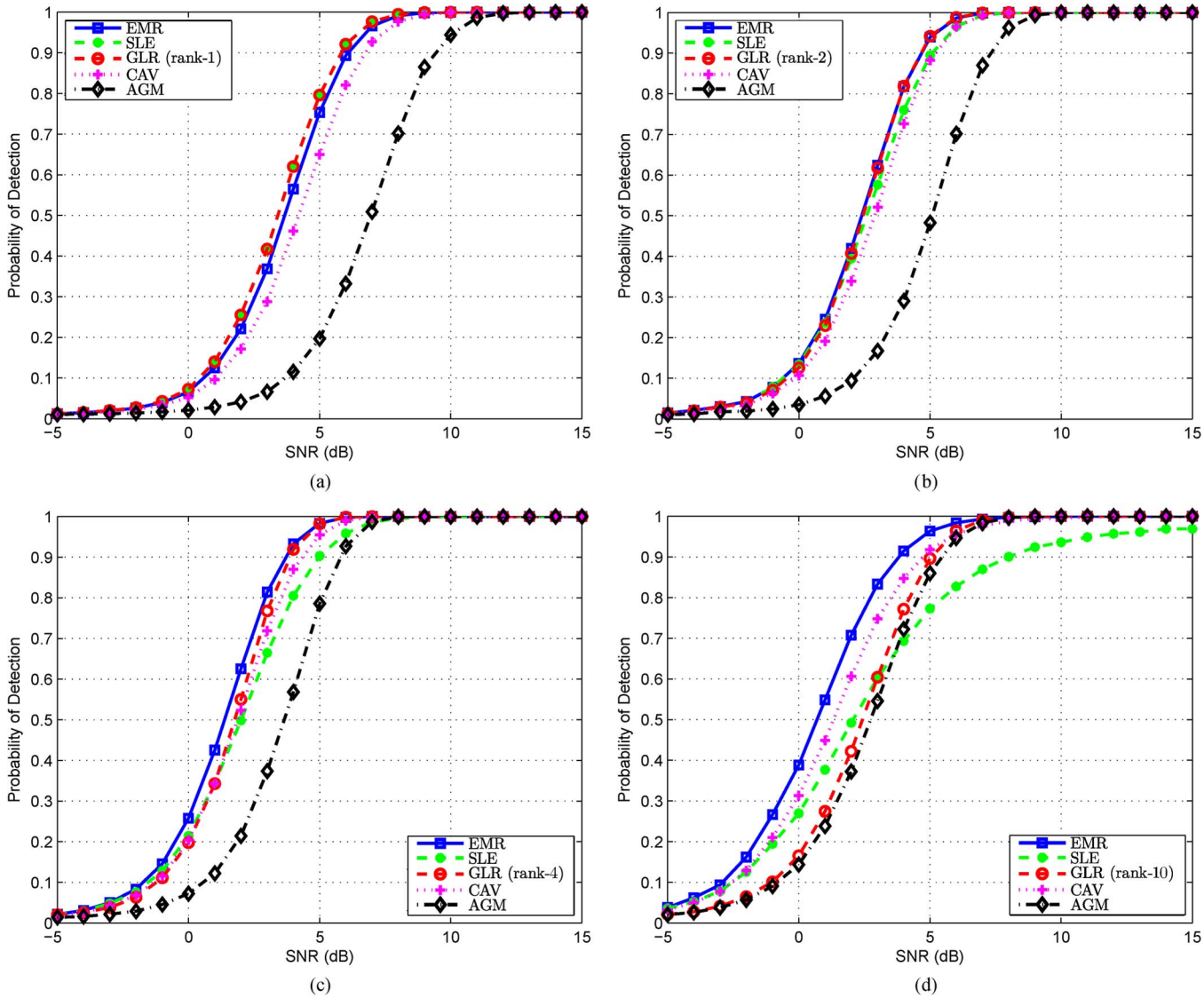

Fig. 3. Probability of detection versus SNR for uncorrelated equal-power primary signals. $m = 12$, $n = 15$, and $P_{\rm fa} = 10^{-2}$. (a) $d = 1$. (b) $d = 2$. (c) $d = 4$. (d) $d = 10$.

the EMR is slightly inferior to the rank-d GLR under the equal-signal-power condition, but this has changed under the unequal-signal-power condition (comparing Fig. 2(c) at SNR $= 8$ dB to Fig. 5(a) at $P_{\rm fa} = 0.01$). These observations are consistent with that obtained in Fig. 4.

Note that the EMR detector also exhibits competitive performance in large-sample cases, which are more commonly encountered in the CR network. As shown in Fig. 6, for a low SNR of -2.5 dB, the EMR performs comparably to the rank-d GLR under both equal-power and Chi-squared distributed power settings. Moreover, the EMR outperforms the AGM, as is consistent with [24], verifying that the EMR is the locally most powerful invariant approach for sphericity test [42].

The strengths and weaknesses for the detection approaches are summarized in Table V. It is implied in Table V that the EMR algorithm is superior to the SLE, CAV, and AGM in detection performance at almost all the conditions. Moreover, although the rank-d GLR approach utilizes the *a priori* information of the primary signal number d, it is still inferior to or comparable with the EMR detector.

As pointed out in Remark 1, in addition to the EMR with $j = 2$, the variant of EMR with a higher moment order j, i.e., $\xi_{\rm EMR}^{(j)}(j \geq 3)$, can also be employed for spectrum sensing. To numerically evaluate the behavior of $\xi_{\rm EMR}^{(j)}(j \geq 3)$, the empirical ROCs of the EMR with different js are plotted in Figs. 7 and 8. More specifically, the results for small samples are shown in Fig. 7, where the number of antennas is six and the number of samples is ten. Moreover, Fig. 7(a) corresponds to the situation of a single primary signal with power of 7 dB, whereas Fig. 7(b) studies the scenario of four primary signals with equal power values of 5 dB. The results for large samples are demonstrated in Fig. 8, in which the number of antennas is six and the number of samples is 100. In Fig. 8(a), there is one primary signal with power of 0 dB. In Fig. 8(b), the number of primary signals is four, and the power for each signal is -3 dB. It is shown in Fig. 7(a) and Fig. 8(a) that the EMR improves as its moment

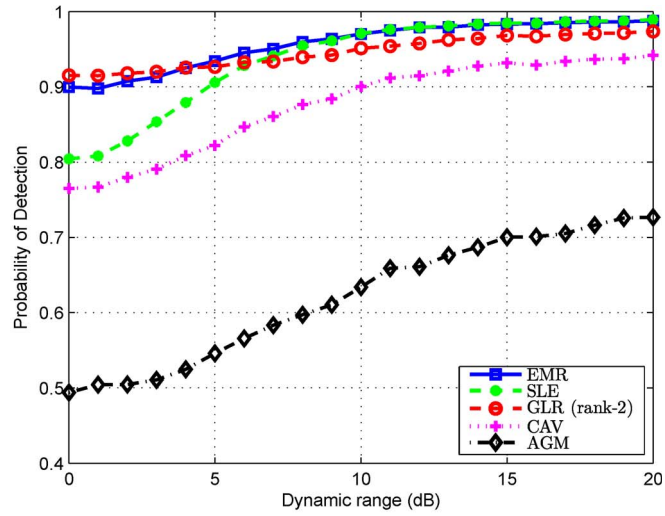

Fig. 4. Probability of detection versus (a) DR of power of $d = 2$ uncorrelated primary signals. (b) CC ρ for $d = 5$ equal-power primary signals. $m = 7$ and $n = 8$, and $P_{\rm fa} = 10^{-2}$. (a) $d = 2$ and SNR $= 7.5$ dB. (b) $d = 5$ and SNR $= 10$ dB.

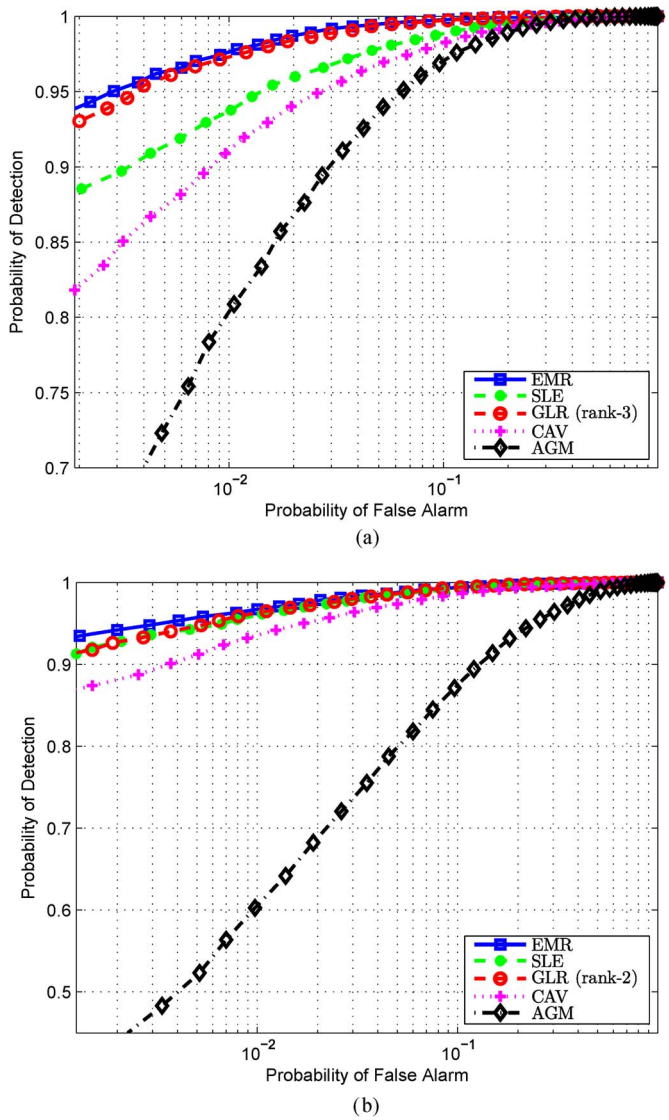

Fig. 5. Empirical ROCs for uncorrelated signals, whose power ratio is randomly drawn from Chi-squared distribution in each Monte Carlo trial. (a) $m = 7$, $n = 8$, $d = 3$, and SNR $= 8$ dB. (b) $m = 12$, $n = 15$, $d = 2$, and SNR $= 5$ dB.

order j increases for the situation of a single primary signal. For multiple primary signals, however, the EMR improves as its moment order j decreases from 6 to 2, as shown in Fig. 7(b) and Fig. 8(b). That is, the performance of the EMR depends on the value of j and the number of primary sources. Thus, the EMR approach has different behaviors from John's detector.

B. Accuracy of Theoretical $P_{\rm fa}$ and P_d

Let us first test the goodness of fit between the theoretical false-alarm probability in (20) and the simulated one. The $P_{\rm fa}$ versus $\gamma_{\rm EMR}$ is plotted in Fig. 9. It is shown in [24] that the approximate beta distribution based on moment matching is able to yield accurate false-alarm probability. As a result, the theoretical $P_{\rm fa}$ derived in [24] is also included for comparison. We observe that theoretical false-alarm probability in (20) agrees well with the simulated one and is comparable to the expression of [24] in accuracy. Nevertheless, neither the false-alarm probability in (20) nor the expression in [24] can accurately fit the empirical false-alarm probability for large thresholds. At large thresholds, the false-alarm probability becomes very small, e.g., less than 10^{-3}. Recall that the false-alarm probability in (20) is based on the asymptotic Gaussian distribution in (19), which has the convergence rate $\mathcal{O}(m^{-2})$. This thereby prohibits the expression in (20) to accurately predict the false-alarm probability at large thresholds. On the other hand, notice that the approximate beta distribution in [24] is based on the first- and second-order moment matching, without considering the higher order moments. Consequently, it cannot provide accurate prediction for the false-alarm probability at large thresholds either.

Indeed, for larger m and n, it may be difficult to accurately calculate the CDF in [24] due to the high numerical precision and large DR required to evaluate the moments in [24, eq. (13)]. Moreover, note that the CDF expression in [24] varies with m and n. This implies that we have to store a large number of

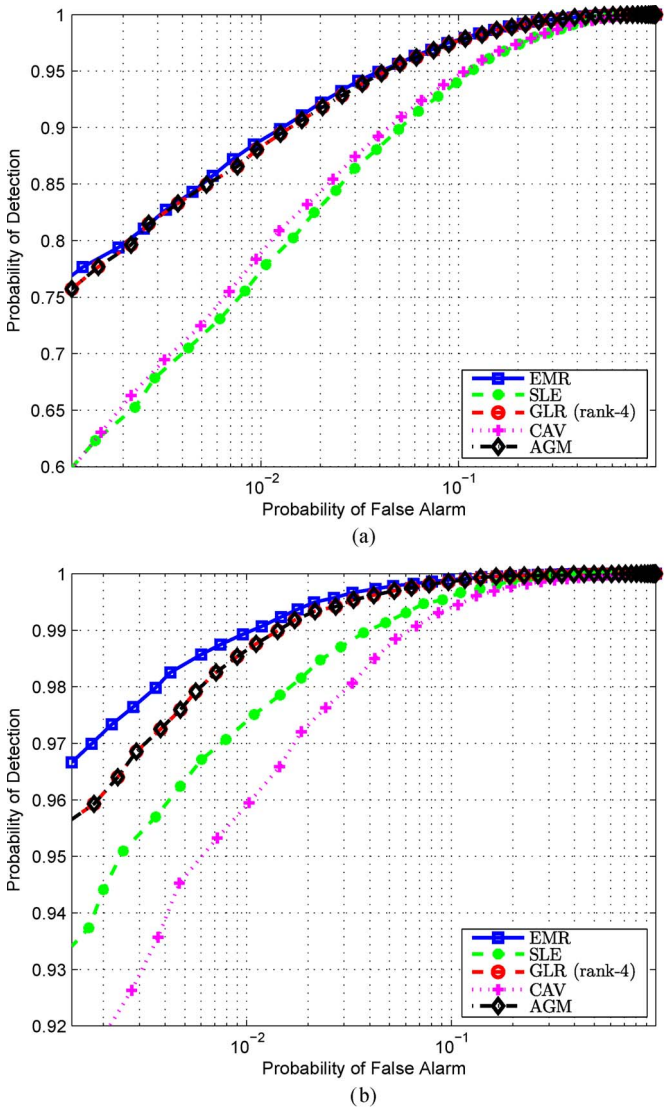

Fig. 6. Empirical ROCs for uncorrelated signals, whose power ratio is randomly drawn from Chi-squared distribution in each Monte Carlo trial. $m = 5$, $n = 100$, $d = 4$, and SNR $= -3$ dB. (a) Equal power. (b) Chi-squared distributed power.

lookup tables (for finding the inverse of the CDF) for every possible pair of m and n, which involves additional storage and renders real-time sensing difficulty particularly when n varies dynamically with time. In contrast, our derived false-alarm probability in (20) is much simpler to evaluate and only involves the Q-function, which is independent of m and n. Therefore, only one lookup table needs to be established at the receiver. Moreover, our expression is more suitable for applications with strict real-time or processing-delay requirements.

Now, let us examine the accuracy of the theoretical detection probability. The theoretical ROCs of the EMR are plotted in Fig. 10, which stands for the mapping between the theoretical false-alarm probability and theoretical detection probability. The empirical ROCs of the EMR are provided as well for the purpose of comparison. For the situation with two PUs shown in Fig. 10(a), the theoretical P_d agrees well with its simulated counterpart when the signal power is well above λ_{DET} or well below λ_{DET}. However, for an intermediate signal power that is close to the λ_{DET}, which is referred to as the transition region [43], an apparent deviation of the theoretical detection probability from its simulated counterpart is observed. In this transition region [43], the fluctuation of the sample eigenvalues becomes difficult to characterize due to the complicated interactions between the noise and signal eigenvalues, which feature the phase transition phenomenon [43]. The derivation of a more accurate formula for the transition region deserves further research and is left as our future work. Note that, for large-sample scenarios, the derived P_d is still able to provide an accurate prediction of the detection performance of the EMR, as shown in Fig. 10(b). Note also that our expression of the detection probability provides comparable accuracy to that derived in [24],[3] which has a more involved form and is hence much more computationally expensive to evaluate.

C. Comparison of Computational Complexity

The computational times for various algorithms are shown in Fig. 11, where the numbers of antennas and samples vary at the same rate, namely, $m/n = 0.8$. Note that the SNR and signal number have no effect on the computational time. We observe that the SLE, rank-2 GLR, MME, and AGM consume almost the same computational time, of which the slight difference is caused by the different extra time required to compute the statistics once the sample eigenvalues have been obtained. Specifically, the rank-2 GLR, AGM, and SLE require slightly more computational time than the MME since they involve additional additions and multiplications of the smallest sample eigenvalues. It is seen that the EMR and CAV need similar computational time, with the slight difference resulting from the extra square root operations in the CAV. Moreover, as m and n increase, the computational times of the AGM/MME/SLE/rank-2 GLR increase most rapidly, followed by the CAV/EMR, and the ED increases the slowest. Thus, the numerical results are consistent with the theoretical calculations in Table III.

V. Conclusion

An EMR algorithm has been devised to handle the blind spectrum sensing in sample-starving environments. In the threshold calculation, the EMR approach is able to use the RMT results on the moments of the noise sample eigenvalues and does not ignore any fluctuation, significantly enhancing the computation accuracy. Moreover, as the EMR detector is derived from the RMT perspective and utilizes all the signal eigenvalues for detection, it outperforms other blind detectors particularly for relatively small-sample scenarios. Furthermore, the detection probability of the EMR method is theoretically produced based on our derived analytical distribution of the EMR statistic in the presence of primary signals. The numerical results agree well with our theoretical analysis.

[3]Note that, in [24, Prop. 4], the mean value μ_z in the denominator of the right-hand side (RHS) of (23a) and (23b) is wrong and has been corrected as the variance ν_z.

TABLE V
SUMMARY OF STRENGTHS AND WEAKNESSES FOR VARIOUS DETECTORS IN TERMS OF DETECTION PERFORMANCE

Detector	$d = 1$, equal power	$d \geq 2$, equal power	small DR/CC	large DR/CC	small n, unequal power	large n, unequal power
EMR	Good	Good	Fair	Good	Good	Good
SLE	Good	Poor	Poor	Fair	Fair	Poor
GLR(rank-d)	Good	Good	Good	Fair	Fair	Fair
CAV	Fair	Fair	Poor	Poor	Fair	Poor
AGM	Poor	Poor	Poor	Poor	Poor	Fair

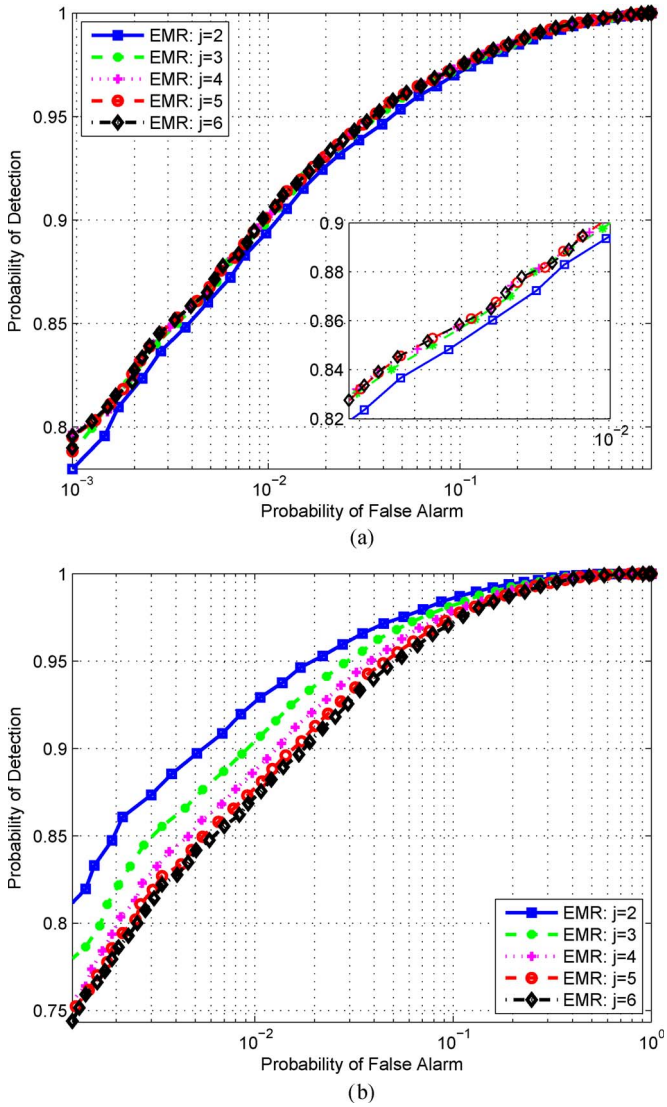

Fig. 7. Empirical ROCs of EMR variants. $m = 6$, $n = 10$. (a) $d = 1$ and SNR $= 7$ dB. (b) $d = 4$, SNR $= 5$ dB, and signals are uncorrelated.

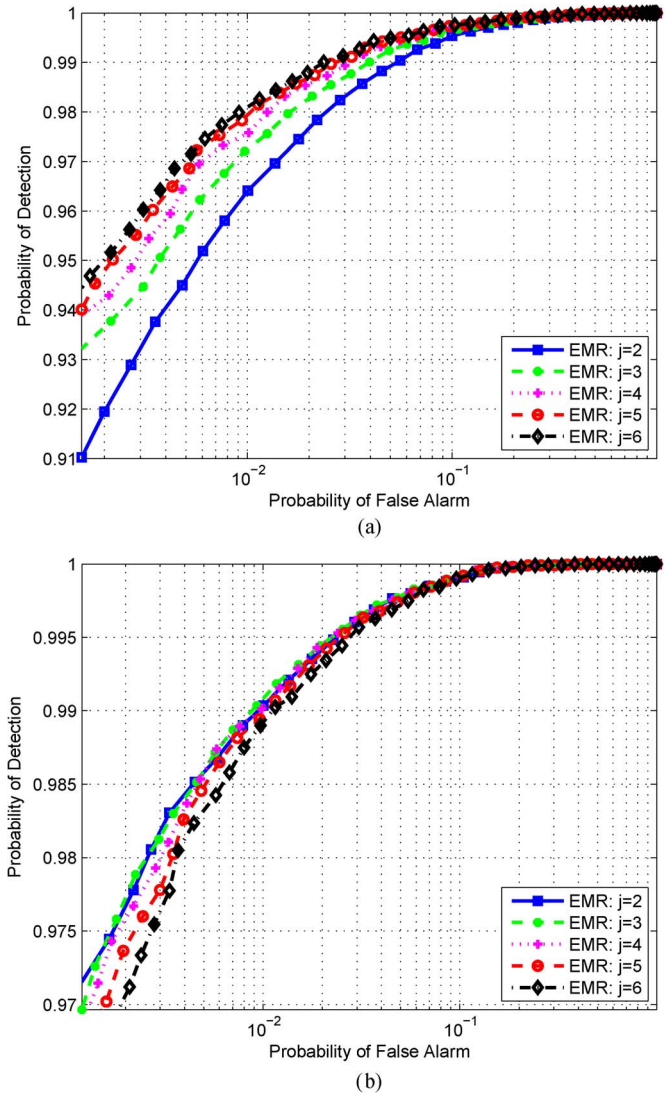

Fig. 8. Empirical ROCs of EMR variants. $m = 6$, and $n = 100$. (a) $d = 1$ and SNR $= 0$ dB. (b) $d = 4$, SNR $= -3$ dB, and signals are uncorrelated.

APPENDIX A
PROOF OF PROPOSITION 2

Setting

$$\bar{\ell}_s \triangleq \sum_{i=1}^{d} \ell_i, \quad \bar{\ell}_w \triangleq \sum_{i=d+1}^{m} \ell_i \tag{36}$$

$$\tilde{\ell}_s \triangleq \sum_{i=1}^{d} \ell_i^2, \quad \tilde{\ell}_w \triangleq \sum_{i=d+1}^{m} \ell_i^2 \tag{37}$$

it follows from (17) that

$$\xi_{\mathrm{EMR}} = m \frac{\tilde{\ell}_s + \tilde{\ell}_w}{(\bar{\ell}_s + \bar{\ell}_w)^2}. \tag{38}$$

For fixed d and signal power values, $\tilde{\ell}_s \ll \tilde{\ell}_w$ and $\bar{\ell}_s \ll \bar{\ell}_w$ as $m, n \to \infty$ with $m/n \to c$; hence, the fluctuation of ξ_{EMR} is dominated by those of $\tilde{\ell}_w$ and $\bar{\ell}_w$. Therefore, we can replace the expressions of $\tilde{\ell}_s$ and $\bar{\ell}_s$ by their limiting values in the joint limit $m, n \to \infty$ with $m/n \to c$.

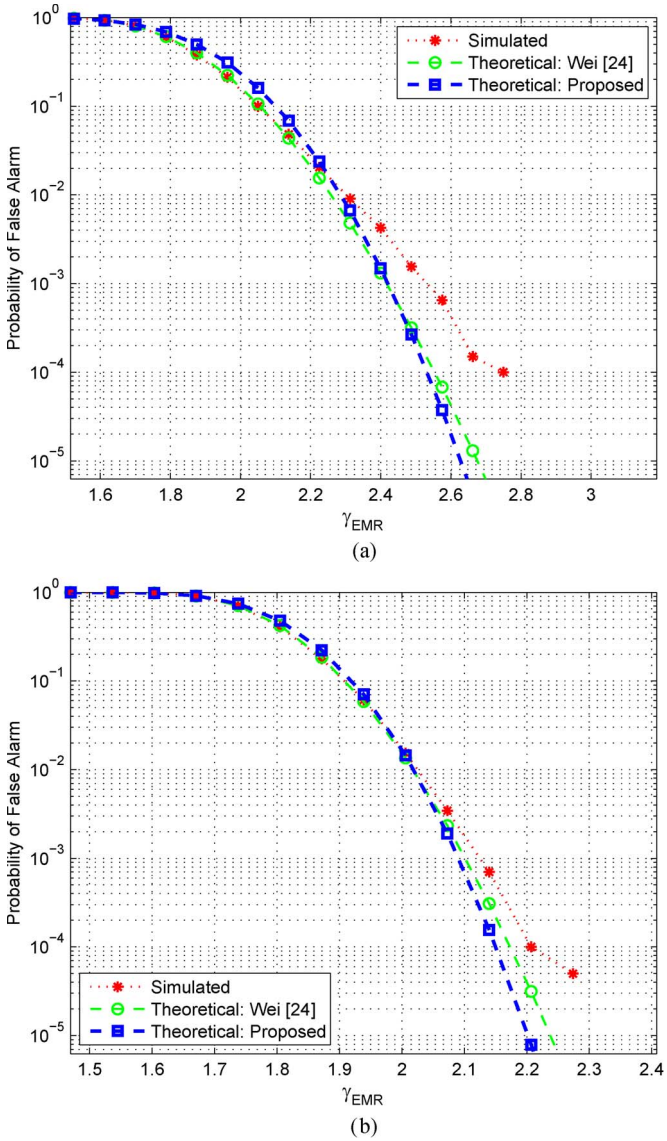

Fig. 9. Test of goodness of agreement between theoretical and simulated false-alarm probabilities. (a) $m = 7$ and $n = 8$. (b) $m = 12$ and $n = 15$.

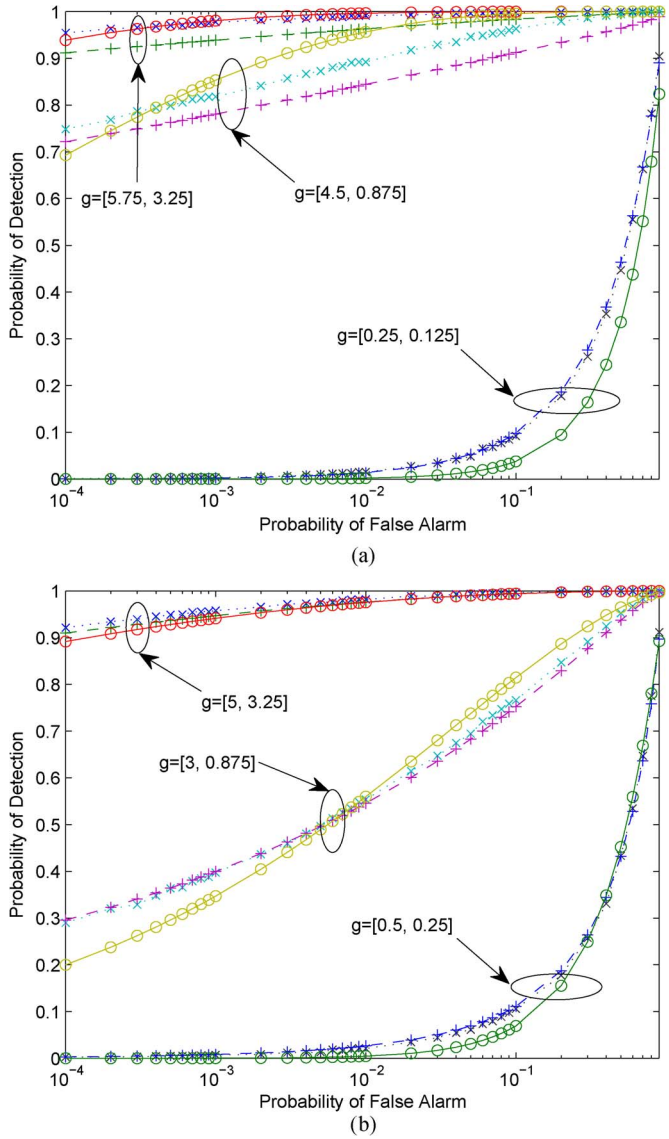

Fig. 10. Test of goodness of agreement between theoretical and simulated probabilities of detection. $d = 2$ PU signals are assumed present, and their power values are expressed as $\sigma_{s_i}^2 = g_i \lambda_{\mathrm{DET}}, i = 1, 2$, where g_i is the scaling coefficient, and λ_{DET} is the asymptotic limit of detection. The dotted line with cross markers corresponds to the simulated detection probability, the dashed line with plus markers represents the theoretical detection probability derived in [24] [see Propositions 3 and 4 and (19)–(24)], and the solid line with circle markers denotes the derived theoretical detection probability of (30) that is obtained from the analytical distribution function of ξ_{EMR} in (25) and (32). (a) $m = 12$ and $n = 15$. (b) $m = 4$ and $n = 60$.

According to [44, Prop. 3.41], as $m, n \to \infty$ and $m/n \to c$, the sample eigenvalue $\ell_i (i = 1, \ldots, d)$, a.s. converges to its limiting value, i.e.,

$$\ell_i \xrightarrow{\text{a.s.}} \mathrm{E}[\ell_i] = (\lambda_i + \tau)\left(1 + \frac{c\tau}{\lambda_i}\right) \tag{39}$$

$$\ell_i^2 \xrightarrow{\text{a.s.}} \mathrm{E}[\ell_i^2] = (\lambda_i + \tau)^2\left(1 + \frac{c\tau}{\lambda_i}\right)^2. \tag{40}$$

It follows that

$$\bar{\ell}_s \xrightarrow{\text{a.s.}} \sum_{i=1}^{d} (\lambda_i + \tau)\left(1 + \frac{c\tau}{\lambda_i}\right) \triangleq \nu_1 \tag{41}$$

$$\tilde{\ell}_s \xrightarrow{\text{a.s.}} \sum_{i=1}^{d} (\lambda_i + \tau)^2\left(1 + \frac{c\tau}{\lambda_i}\right)^2 \triangleq \nu_2. \tag{42}$$

Substituting (41) and (42) into (38) yields

$$\xi_{\mathrm{EMR}} \to m \frac{\nu_2 + \tilde{\ell}_w}{(\nu_1 + \bar{\ell}_w)^2}. \tag{43}$$

On the other hand, since $\lambda_i > \sqrt{c}\tau$, $i = 1, \ldots, d$, the interaction between the signal and noise eigenvalues are small (See (3.23) and the interacting particle system interpretation of the sample eigenvalues in [44]).[4] Therefore, the limiting distributions of $\bar{\ell}_w$ and $\tilde{\ell}_w$ can be approximated by those in the

[4]When $\lambda_i > \sqrt{c}\tau$, $i = 1, \ldots, d$, it holds that $\ell_i \gg \ell_j$, $i = 1, \ldots, d$, $j = d+1, \ldots, m$; therefore $L_{\mathrm{Spk}}(\ell_1, \ldots, \ell_d | \ell_{d+1}, \ldots, \ell_m)$ in [44, (3.23)] is approximately independent of the noise eigenvalues $\ell_{d+1}, \ldots, \ell_m$. It follows that the marginal probability density function of the noise sample eigenvalues $\ell_{d+1} \geq \cdots \geq \ell_m$, which is deduced by integrating out $\ell_1, \ldots, \ell_d$ from the joint probability density, is approximately equal to $L_{\mathrm{Bulk}}(\ell_{d+1}, \ldots, \ell_m)$. $L_{\mathrm{Bulk}}(\ell_{d+1}, \ldots, \ell_m)$ turns out to be the same form as the probability density function of "noise" eigenvalues in the absence of signals.

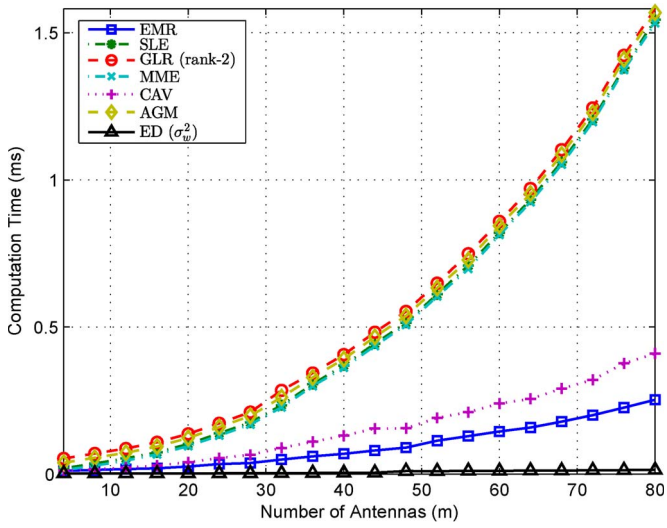

Fig. 11. Computational time versus the number of antennas m. $m/n = 0.8$.

absence of signals. According to [27] and [37], in the absence of signals, the vector $\boldsymbol{z} \triangleq [\bar{\ell}_w - (m-d)\tau, \tilde{\ell}_w - (m-d)\tau^2(1+c)]^T$ tends to be Gaussian distributed, i.e.,

$$\boldsymbol{z} \xrightarrow{\mathcal{D}} \mathcal{N}(\mathbf{0}_2, \boldsymbol{D}) \tag{44}$$

where $\mathbf{0}_2 = [0,0]^T$ and $\boldsymbol{D}$ is defined in (29a). It is worth pointing out that the proof of the limiting fluctuation of $\boldsymbol{z}$ in (44) was first conducted in [26] for real-valued observation and later on in [37] for complex-valued observation, and the results were well summarized in [27].

To determine the distribution of ξ_{EMR} by means of the Delta method, we set $f(x,y) = m(\nu_2 + y)/(\nu_1 + x)^2$ with $x = \bar{\ell}_w$ and $y = \tilde{\ell}_w$. Applying the first-order Taylor series expansion of $f(x,y)$ around $(x_0, y_0) = ((m-d)\tau, (m-d)\tau^2(1+c))$, we obtain

$$\begin{aligned} f(x,y) &\simeq f(x_0,y_0) + \partial f_x(x_0,y_0)(x-x_0) \\ &\quad + \partial f_y(x_0,y_0)(y-y_0) \\ &\simeq f(x_0,y_0) + \boldsymbol{\nabla}^T \boldsymbol{z} \end{aligned} \tag{45}$$

where

$$\boldsymbol{\nabla} = \begin{bmatrix} \partial f_x(x_0,y_0) \\ \partial f_y(x_0,y_0) \end{bmatrix} \tag{46}$$

which, after being simplified, takes the form of (29b). Thus, it follows from (44) and (45) that, as $m, n \to \infty$ and $m/n \to c$, $\xi_{\mathrm{EMR}} - f(x_0,y_0) \xrightarrow{\mathcal{D}} \mathcal{N}(0, \sigma_\xi^2)$, where σ_ξ^2 is shown in (27). This completes the proof.

Appendix B
Proof of Proposition 3

Here, we only outline the proof.

In the presence of unidentifiable (weak) signals $\lambda_i \le \lambda_{\mathrm{DET}}$, $i = q+1, \ldots, d$, the $(d-q)$ smallest signal-plus-noise sample eigenvalues, namely, ℓ_i, $i = q+1, \ldots, d$, can arbitrarily approach the largest noise-only sample eigenvalues as $m, n \to \infty$ and $m/n \to c$ [45]. Due to the interaction between the signal and noise eigenvalues [44], the limiting distributions of $\bar{\ell}_w$ and $\tilde{\ell}_w$ can no longer be well approximated by (44).

To handle that, by noticing that $\lambda_1 \ge \cdots \ge \lambda_q > \lambda_{\mathrm{DET}}$ and hence the interaction between the largest q signal eigenvalues and noise eigenvalues is small [44], the limiting distributions of

$$\bar{l}_w \triangleq \sum_{i=q+1}^{m} \ell_i, \quad \tilde{l}_w \triangleq \sum_{i=q+1}^{m} \ell_i^2 \tag{47}$$

can still be well approximated by (44). Notice that $\bar{l}_w$ and $\tilde{l}_w$ include contributions from the $(d-q)$ weak signal components, namely

$$\bar{l}_w \simeq \sum_{i=q+1}^{m} \breve{\ell}_i + \sum_{i=q+1}^{d} \lambda_i \tag{48}$$

$$\tilde{l}_w \simeq \sum_{i=q+1}^{m} \breve{\ell}_i^2 + \sum_{i=q+1}^{d} \left(\lambda_i^2 + 2\tau\lambda_i\right) \tag{49}$$

where $\{\breve{\ell}_i\}_{i=q+1}^{m}$ are the assumed $(m-q)$ smallest "signal-free" sample eigenvalues, and $\sum_{i=q+1}^{d} \lambda_i$ and $\sum_{i=q+1}^{d}(\lambda_i^2 + 2\tau\lambda_i)$ constitute the contributions of the $(d-q)$ weak signal components. As a result, we first subtract the signal components from $\bar{l}_w$ and $\tilde{l}_w$ and then use (44) to approximate the distribution of the difference.

References

[1] Fed. Commun. Comm., Spectrum policy task force report, Washington DC, USA, Tech. Rep. ET Docket 02-135, Nov. 2002.

[2] J. Mitola, III, "Cognitive radio for flexible mobile multimedia communications," in *Proc. IEEE Int. Workshop MoMuC*, San Diego, CA, USA, Nov. 1999, pp. 3–10.

[3] J. Lundén, V. Koivunen, A. Huttunen, and H. V. Poor, "Collaborative cyclostationary spectrum sensing for cognitive radio systems," *IEEE Trans. Signal Process.*, vol. 57, no. 11, pp. 4182–4195, Nov. 2009.

[4] H. S. Chen, W. Gao, and D. G. Daut, "Signature based spectrum sensing algorithms for IEEE 802.22 WRAN," in *Proc. IEEE ICC*, Glasgow, U.K., Jun. 2007, pp. 6487–6492.

[5] H. Urkowitz, "Energy detection of unknown deterministic signals," *Proc. IEEE*, vol. 55, no. 4, pp. 523–531, Apr. 1967.

[6] Y. Zeng and Y. C. Liang, "Spectrum-sensing algorithms for cognitive radio based on statistical covariances," *IEEE Trans. Veh. Technol.*, vol. 58, no. 4, pp. 1804–1815, May 2009.

[7] R. Zhang and Y. C. Liang, "Exploiting multi-antennas for opportunistic spectrum sharing in cognitive radio networks," *IEEE J. Sel. Topics Signal Process.*, vol. 2, no. 1, pp. 88–102, Feb. 2008.

[8] Y. Zeng and Y. C. Liang, "Eigenvalue-based spectrum sensing algorithms for cognitive radio," *IEEE Trans. Commun.*, vol. 57, no. 6, pp. 1784–1793, Jun. 2009.

[9] A. Taherpour, M. Nasiri-Kenari, and S. Gazor, "Multiple antenna spectrum sensing in cognitive radios," *IEEE Trans. Wireless Commun.*, vol. 9, no. 2, pp. 814–823, Nov. 2010.

[10] P. Wang, J. Fang, N. Han, and H. Li, "Multiantenna-assisted spectrum sensing for cognitive radio," *IEEE Trans. Veh. Technol.*, vol. 59, no. 4, pp. 1791–1800, May 2010.

[11] A. Kortun, T. Ratnarajah, M. Sellathurai, C. Zhong, and C. B. Papadias, "On the performance of eigenvalue-based cooperative spectrum sensing for cognitive radio," *IEEE J. Sel. Topics Signal Process.*, vol. 5, no. 1, pp. 49–55, Feb. 2011.

[12] P. Bianchi, M. Debbah, M. Maïda, and J. Najim, "Performance of statistical tests for single-source detection using random matrix theory," *IEEE Trans. Inf. Theory*, vol. 57, no. 4, pp. 2400–2419, Apr. 2011.

[13] T. J. Lim, R. Zhang, Y. C. Liang, and Y. H. Zeng, "GLRT-based spectrum sensing for cognitive radio," in *Proc. IEEE GLOBECOM*, New Orleans, LA, USA, Dec. 2008, pp. 1–5.

[14] R. Wang and M. Tao, "Blind spectrum sensing by information theoretic criteria for cognitive radios," *IEEE Trans. Veh. Technol.*, vol. 59, no. 8, pp. 3806–3817, Oct. 2010.

[15] R. Zhang, T. Lim, Y. C. Liang, and Y. Zeng, "Multi-antenna based spectrum sensing for cognitive radios: A GLRT approach," *IEEE Trans. Commun.*, vol. 58, no. 1, pp. 84–88, Jan. 2010.
[16] L. Wei and O. Tirkkonen, "Spectrum sensing in the presence of multiple primary users," *IEEE Trans. Commun.*, vol. 60, no. 5, pp. 1268–1277, May 2012.
[17] D. Ramírez, G. Vazquez-Vilar, R. López-Valcarce, J. Vía, and I. Santamaría, "Detection of rank-P signals in cognitive radio networks with uncalibrated multiple antennas," *IEEE Trans. Signal Process.*, vol. 59, no. 8, pp. 3764–3774, Aug. 2011.
[18] S. John, "Some optimal multivariate tests," *Biometrika*, vol. 58, no. 1, pp. 123–127, Apr. 1971.
[19] O. Ledoit and M. Wolf, "Some hypothesis tests for the covariance matrix when the dimension is large compared to the sample size," *Ann. Stat.*, vol. 30, no. 4, pp. 1081–1102, 2002.
[20] R. J. Muirhead, *Aspects of Multivariate Statistical Theory*. New York, NY, USA: Wiley, 1982.
[21] L. Wei, M. McKay, and O. Tirkkonen, "Exact Demmel condition number distribution of complex Wishart matrices via the Mellin transform," *IEEE Commun. Lett.*, vol. 15, no. 2, pp. 175–177, Feb. 2011.
[22] R. López-Valcarce, G. Vazquez-Vilar, and J. Sala, "Multiantenna spectrum sensing for cognitive radio: Overcoming noise uncertainty," in *Proc. 2nd Int. Workshop CIP*, Elba Island, Italy, Jun. 2010, pp. 310–315.
[23] D. Romero and R. Lopez-Valcarce, "Distributed spectrum sensing with multiantenna sensors under calibration errors," in *Proc. IEEE 12th Int. Workshop SPAWC*, San Francisco, CA, USA, Jun. 2011, pp. 441–445.
[24] L. Wei, P. Dharmawansa, and O. Tirkkonen, "Multiple primary user spectrum sensing in the low SNR regime," *IEEE Trans. Commun.*, vol. 61, no. 5, pp. 1720–1731, May 2013.
[25] K. Johansson, "On fluctuations of random Hermitian matrices," *Duke Math. J.*, vol. 91, no. 1, pp. 151–203, 1998.
[26] D. Jonsson, "Some limit theorems for the eigenvalues of a sample covariance matrix," *J. Multivariate Anal.*, vol. 12, no. 1, pp. 1–38, Mar. 1982.
[27] R. R. Nadakuditi and A. Edelman, "Sample eigenvalue based detection of high-dimensional signals in white noise using relatively few samples," *IEEE Trans. Signal Process.*, vol. 56, no. 7, pp. 2625–2638, Jul. 2008.
[28] S. M. Kay, *Fundamentals of Statistical Signal Processing: Detection Theory*, vol. 2. Englewood Cliffs, NJ, USA: Prentice-Hall, 1998.
[29] R. Tandra and A. Sahai, "SNR walls for signal detection," *IEEE J. Sel. Topics Signal Process.*, vol. 2, no. 1, pp. 4–17, Feb. 2008.
[30] I. M. Johnstone, "High dimensional statistical inference and random matrices," in *Proc. Int. Congr. Math.*, 2006, pp. 307–333.
[31] Q. T. Zhang, "Advanced detection techniques for cognitive radio," in *Proc. IEEE ICC*, Dresden, Germany, Jun. 2009, pp. 1–5.
[32] L. Wei, O. Tirkkonen, P. Dharmawansa, and M. McKay, "On the exact distribution of the scaled largest eigenvalue," in *Proc. IEEE ICC*, Ottawa, ON, Canada, Jun. 2012, pp. 2422–2426.
[33] A. Kortun, M. Sellathurai, T. Ratnarajah, and C. Zhong, "Distribution of the ratio of the largest eigenvalue to the trace of complex Wishart matrices," *IEEE Trans. Signal Process.*, vol. 60, no. 10, pp. 5527–5532, Oct. 2012.
[34] F. Bornemann, "On the numerical evaluation of distributions in random matrix theory: A review," *Markov Process. Related Fields*, vol. 16, no. 4, pp. 803–866, 2010.
[35] J. W. Silverstein, "Large dimensional random matrix theory for signal detection and estimation in array processing," in *Proc. IEEE 6th SP Workshop Statist. Signal Array Process.*, Victoria, BC, Canada, Oct. 1992, pp. 276–279.
[36] V. A. Marčenko and L. A. Pastur, "Distribution of eigenvalues in certain sets of random matrices," *Math. Sb. (N.S.)*, vol. 72, no. 114, pp. 507–536, 1967.
[37] Z. D. Bai and J. W. Silverstein, "CLT for linear spectral statistics of large-dimensional sample covariance matrices," *Ann. Probability*, vol. 32, no. 1A, pp. 553–605, Jan. 2004.
[38] H. Cremér, *Mathematical Methods of Statistics*, vol. 9. Princeton, NJ, USA: Princeton Univ. Press, 1999.
[39] S. J. Shellhammer, "Spectrum sensing in IEEE 802.22," in *Proc. IAPR Workshop CIP*, Santorini, Greece, Jun. 9–10, 2008, pp. 1–6.
[40] R. Tandra and A. Sahai, "Fundamental limits on detection in low SNR under noise uncertainty," in *Proc. Int. Conf. Wireless Netw., Commun. Mobile Comput.*, Maui, HI, USA, Jun. 2005, vol. 1, pp. 464–469.
[41] A. Onatski, M. J. Moreira, and M. Hallin, "Signal detection in high dimension: The multispiked case," *Ann. Statist.*, vol. 42, no. 1, pp. 225–254, 2014.
[42] N. Sugiura, "Locally best invariant test for sphericity and the limiting distributions," *Ann. Math. Statist.*, vol. 43, no. 4, pp. 1312–1316, Aug. 1972.
[43] J. Baik, G. Ben Arous, and S. Péché, "Phase transition of the largest eigenvalue for nonnull complex sample covariance matrices," *Ann. Probability*, vol. 33, no. 5, pp. 1643–1697, Sep. 2005.
[44] R. R. Nadakuditi, "Applied stochastic Eigen-analysis," M.S. thesis, Mass. Inst. Technol., Cambridge, MA, USA, Feb., 2007.
[45] J. Baik and J. W. Silverstein, "Eigenvalues of large sample covariance matrices of spiked population models," *J. Multivariate Anal.*, vol. 97, no. 6, pp. 1382–1408, 2006.

Lei Huang (M'07) was born in Guangdong, China. He received the B.Sc., M.Sc., and Ph.D. degrees from Xidian University, Xian, China, in 2000, 2003, and 2005, respectively, all in electronic engineering.

From 2005 to 2006, he was a Research Associate with the Department of Electrical and Computer Engineering, Duke University, Durham, NC, USA. From 2009 to 2010, he was a Research Fellow with the Department of Electronic Engineering, City University of Hong Kong, Kowloon, Hong Kong, and a Research Associate with the Department of Electronic Engineering, The Chinese University of Hong Kong, Shatin, Hong Kong. Since 2011, he has been with the Department of Electronic and Information Engineering, Harbin Institute of Technology Shenzhen Graduate School, Shenzhen, China, where he is currently a Professor. His research interests include spectral estimation, array signal processing, and statistical signal processing, as well as their applications in radar and wireless communication systems.

Dr. Huang is currently an Editorial Board Member of *Digital Signal Processing*.

Jun Fang (M'08) received the B.S. and M.S. degrees from Xidian University, Xian, China, in 1998 and 2001, respectively, and the Ph.D. degree from the National University of Singapore, Singapore, in 2006, all in electrical engineering.

In 2006, he was a Postdoctoral Research Associate with the Department of Electrical and Computer Engineering, Duke University, Durham, NC, USA. From January 2007 to December 2010, he was a Research Associate with the Department of Electrical and Computer Engineering, Stevens Institute of Technology, Hoboken, NJ, USA. Since January 2011, he has been with the University of Electronic of Science and Technology of China, Chengdu, China. His current research interests include statistical signal processing, sparse theory and compressed sensing, and Bayesian statistical inference.

Dr. Fang received the IEEE Vehicular Technology Society Jack Neubauer Memorial Award in 2013 and the IEEE Africon Outstanding Paper Award in 2011. He currently serves as an Associate Technical Editor for IEEE COMMUNICATIONS MAGAZINE and as an Associate Editor for IEEE SIGNAL PROCESSING LETTERS.

Kefei Liu received the B.Sc. degree in mathematics and the Ph.D. degree in electronic engineering from Wuhan University, Wuhan, China, in 2006 and the City University of Hong Kong, Kowloon, Hong Kong, in 2013. His Ph.D. supervisor was Prof. H.-C. So, and his Ph.D. research topics were statistical and array signal processing, source enumeration, direction-of-arrival estimation, and multilinear algebra.

From September 2013 to December 2013, he was a Research Assistant for Prof. L. Huang with the Department of Electronic and Information Engineering, Harbin Institute of Technology Shenzhen Graduate School, Shenzhen, China. Since January 2014, he has been a Postdoctoral Research Associate with the Department of Computer Science and Engineering and the Center for Evolutionary Medicine and Informatics of the Biodesign Institute, Arizona State University, Tempe, AZ, USA. His cooperative supervisor is Prof. J. Ye. His current research interests include tensor decompositions for machine learning and randomized algorithms for matrix approximation, as well as their applications for the analysis of massive biomedical data sets.

Hing Cheung So (S'90–M'95–SM'07) was born in Hong Kong. He received the B.Eng. degree in electronic engineering from the City University of Hong Kong, Kowloon, Hong Kong, in 1990 and the Ph.D. degree in electronic engineering from The Chinese University of Hong Kong, Shatin, Hong Kong, in 1995, respectively.

From 1990 to 1991, he was an Electronic Engineer with the Research and Development Division, Everex Systems Engineering Ltd., Hong Kong. From 1995 to 1996, he was a Postdoctoral Fellow with The Chinese University of Hong Kong. From 1996 to 1999, he was a Research Assistant Professor with the Department of Electronic Engineering, City University of Hong Kong, where he is currently an Associate Professor. His research interests include statistical signal processing, fast and adaptive algorithms, signal detection, parameter estimation, and source localization.

Dr. So was an Associate Editor for IEEE TRANSACTIONS ON SIGNAL PROCESSING during 2010–2014. He is currently on the editorial boards of the IEEE SIGNAL PROCESSING MAGAZINE, *Signal Processing*, and *Digital Signal Processing*. He is a member of the Signal Processing Theory and Methods Technical Committee of the IEEE Signal Processing Society.

Hongbin Li (M'99–SM'08) received the B.S. and M.S. degrees from the University of Electronic Science and Technology of China in 1991 and 1994, respectively, and the Ph.D. degree from the University of Florida, Gainesville, FL, USA, in 1999, all in electrical engineering.

From July 1996 to May 1999, he was a Research Assistant with the Department of Electrical and Computer Engineering, University of Florida. Since July 1999, he has been with the Department of Electrical and Computer Engineering, Stevens Institute of Technology, Hoboken, NJ, USA, where he is currently a Professor. In the summers of 2003, 2004, and 2009, he was a Summer Visiting Faculty Member with the Air Force Research Laboratory. His main research interests include statistical signal processing, wireless communications, and radars.

Dr. Li has been a member of the IEEE Signal Processing Society (SPS) Signal Processing Theory and Methods (2011–present) Technical Committee (TC) and the IEEE SPS Sensor Array and Multichannel TC (2006–2012). He is an Associate Editor for *Elsevier Signal Processing* and served on the editorial boards for IEEE TRANSACTIONS ON WIRELESS COMMUNICATIONS, IEEE SIGNAL PROCESSING LETTERS, and the IEEE TRANSACTIONS ON SIGNAL PROCESSING. He was a Guest Editor for the *EURASIP Journal on Applied Signal Processing*. He has been involved in various conference organization activities, including serving as a General Co-Chair for the Seventh IEEE Sensor Array and Multichannel Signal Processing (SAM) Workshop, Hoboken, June 17–20, 2012. He received the IEEE Jack Neubauer Memorial Award in 2013 for the best systems paper published in the IEEE TRANSACTIONS ON VEHICULAR TECHNOLOGY, the Outstanding Paper Award from the IEEE AFICON Conference in 2011, the Harvey N. Davis Teaching Award in 2003, the Jess H. Davis Memorial Award for excellence in research in 2001 from Stevens Institute of Technology, and the Sigma Xi Graduate Research Award from the University of Florida in 1999. He is a member of Tau Beta Pi and Phi Kappa Phi.